# PV-POWERED MEMBRANE SYSTEM CONTROL FOR CONTINUOUS AUTONOMOUS WATER SOLUTION IN REMOTE AREAS

A THESIS SUBMITTED IN PARTIAL FULFILLMENT OF

THE REQUIREMENTS FOR THE DEGREE OF

MASTER OF SCIENCE IN RENEWABLE ENERGY

OF

THE UNIVERSITY OF NAMIBIA

BY

RAUNA NDAPANDULA KASHEETA

201603378

APRIL 2025

MAIN SUPERVISOR: DR. PETJA DOBREVA

(UNIVERSITY OF NAMIBIA)

CO-SUPERVISOR: PROF. BRYCE S. RICHARDS

(KARLSRUHE INSTITUTE OF TECHNOLOGY)

## Abstract

This research addressed the challenge of Solar Irradiance (SI) fluctuations, which adversely affect the performance of photovoltaic-membrane (PV-membrane) systems used for water purification. These fluctuations lead to reduced permeate volume and quality, as well as increased specific energy consumption. The primary aim of this research is to incorporate mechanical energy storage and develop a hydraulic buffering control method to enhance system performance under varying SI conditions. To achieve this, a hydraulic energy storage system utilizing a bladder tank was implemented, designed to buffer periods of SI fluctuations. A control algorithm was developed that allows the hydraulic bladder accumulator to discharge during low solar irradiance periods for buffering and charge during high solar irradiance periods by monitoring power ramp-down rates. Results indicate that, in the worst-case scenario of a very cloudy day, the system produced an additional 98.5 L of permeate while maintaining permeate quality within the WHO palatable limit of 1.13 mS/cm. Furthermore, the average specific energy consumption was reduced by 38%. The algorithm effectively prevented system pressure from dropping to zero, thereby maintaining system stability despite fluctuations caused by SI changes. Future investigations should focus on minimizing pump shutdowns during hydraulic buffering due to increased pressure resistance. This research contributes to sustainable water solutions in remote areas, offering a promising approach to enhance the reliability and efficiency of PV-powered membrane systems.

**List of Conference(s) Proceedings**

- Kasheeta, R. N. (2024). PV-powered Membrane System Control for a Sustained Water Solution in Remote Areas. Proceedings of the JCoI Youth for Green Hydrogen (Y4H2) Scholarship Programme Visibility Event - Germany and Namibia Partnership. Berlin, Germany.

**Table of Contents**

**List of Tables**

**List of Figures**

**List of Abbreviations and/or Acronyms**

| | |
|---|---|
| - | Negative |
| " | Inch |
| **%** | Percent |
| ~ | Approximately |
| + | Positive |
| < | Less than |
| = | Equal to |
| > | Greater than |
| ± | Plus-minus |
| ≤ | Less than or equal to |
| **°F** | Degree Fahrenheit |
| **A** | Ampere |
| **AC** | Alternating Current |
| **°C** | Degree Celsius |
| **DC** | Direct Current |
| **DIN** | Deutsches Institut für Normung |
| **DoD** | Depth of Discharge |
| **EC** | Electrical Conductivity |
| **ED** | Electrodialysis |
| **FS** | Full Scale |
| **$ft^2$** | Square feet |
| **g/L** | Grams per Litre |

| | |
|---|---|
| **gpd** | Gallons per day |
| **HMI** | Human Machine Interface |
| **Hz** | Hertz |
| **I/O** | Input/Output |
| **I-V** | Current-Voltage |
| **kg/m$^3$** | Kilogram per cubic metre |
| **KIT** | Karlsruhe Institute of Technology |
| **kW** | Kilowatt |
| **L** | Litre |
| **L/h.m$^2$** | Litres per hour per square metre |
| **L/min** | Litre per minute |
| **LA** | Lead-Acid |
| **Li-ion** | Lithium-ion |
| **m/s** | Metres per second |
| **m$^2$** | Square metre |
| **m$^3$/d** | Cubic metre per day |
| **m$^3$/h** | Cubic metre per hour |
| **mA** | Milliampere |
| **max.** | Maximum |
| **MCr** | Membrane Crystallization |
| **MD** | Membrane Distillation |
| **min.** | Minimum |
| **MPPT** | Maximum Power Point Tracker |
| **mS/cm** | Millisiemens per Centimetre |

| | |
|---|---|
| **NaCl** | Sodium Chloride |
| **NBR** | Nitrile Butadiene Rubber |
| **NC** | Normally Closed |
| **NF** | Nanofiltration |
| **nm** | Nanometre |
| **non-cond.** | Non-conductive |
| **PCB-ETFE** | Printed Circuit Board-Ethylene Tetrafluoroethylene |
| **PLC** | Programmable Logic Controller |
| $\mathbf{P_{max}}$ | Maximum pressure |
| $\mathbf{P_{min}}$ | Minimum pressure |
| $\mathbf{P_{set}}$ | Set operating pressure |
| **psi** | Pounds per square inch |
| **PV** | Pervaporation |
| **PV** | Photovoltaic |
| **RE** | Renewable Energy |
| **RH** | Relative Humidity |
| **RISC** | Reduced Instruction Set Computer |
| **RO** | Reverse Osmosis |
| **rpm** | Revolutions per minute |
| **SC** | Supercapacitor |
| **SEC** | Specific Energy Consumption |
| **SI** | Solar Irradiance |
| **SWRO** | Small-scale Seawater Reverse Osmosis |
| **TDS** | Total Dissolved Salts |

| | |
|---|---|
| **UF** | Ultrafiltration |
| **uni-/bipolar** | Universal/bipolar |
| **V** | Volt |
| **VAC** | Volts Alternating Current |
| **VDC** | Volts Direct Current |
| **W** | Watt |
| **Wh/L** | Watt-hours per litre |
| **WHO** | World Health Organization |
| **µm** | Micrometre |
| **µS/cm** | Microsiemens per centimetre |
| **Ω** | Ohm |

**Acknowledgments**

I would like to express my heartfelt gratitude to all those who contributed to the successful completion of this research. Firstly, I extend my sincere appreciation to my supervisors, Dr. Petja Dobreva, Mr. Emmanuel O. Ogunniyi, and Prof. Bryce S. Richards. Their unwavering support, expert guidance, and constructive feedback were invaluable throughout my research journey. Their mentorship not only enriched my academic experience but also inspired me to strive for excellence in my work.

I would also like to acknowledge the institutions that played a crucial role in facilitating this research: the University of Namibia (UNAM) and the Karlsruhe Institute of Technology (KIT). The resources, facilities, and collaborative environment provided by both institutions significantly enhanced the quality of my research and learning experience.

Furthermore, I am deeply grateful for the support from various organizations that made this study possible for the scholarship funding. I would like to thank the government of the Republic of Namibia for its commitment to advancing education and research in the country. My appreciation also extends to the Federal Ministry of Education and Research (BMBF) in Germany for their support, as well as the Southern African Science Service Centre for Climate Change and Adaptive Land Management (SASSCAL). Additionally, I am thankful to the German Academic Exchange Service (DAAD) for providing scholarship funding that enabled me to pursue my research in Germany.

Lastly, I would like to express my heartfelt thanks to my family and friends for their support and encouragement during my academic journey. Their belief in me and their continuous mental support have been a source of strength and motivation throughout this process. This research is a testament to the collective efforts of all these individuals and institutions, and I am truly grateful for their contributions to my success.

**Declarations**

I, Rauna Ndapandula Kasheeta, hereby declare that this study is my own work and is a true reflection of my research, and that this work, or any part thereof has not been submitted for a degree at any other institution. No part of this thesis/dissertation may be reproduced, stored in any retrieval system, or transmitted in any form, or by means (e.g. electronic, mechanical, photocopying, recording or otherwise) without the prior permission of the author, or The University of Namibia in that behalf.

I, Rauna Ndapandula Kasheeta, grant The University of Namibia the right to reproduce this thesis in whole or in part, in any manner or format, which The University of Namibia may deem fit.

| | | |
|---|---|---|
| **Rauna Ndapandula Kasheeta** | 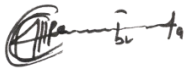 | **31/10/2024** |
| …….. | …… | …… |
| Name of Student | Signature | Date |

# 1. INTRODUCTION

## 1.1. Background of the Study

Access to clean and safe drinking water remains a critical challenge in many low-income countries, particularly in remote and off-grid areas[1,2]. As global clean water scarcity intensifies due to population growth, climate change, and increasing urbanisation, the need for sustainable and cost-effective water treatment solutions has become more pressing [2,3]. Photovoltaic-membrane (PV-membrane) desalination technology is a promising solution for providing potable water in decentralised (small-scale) systems where conventional infrastructure is lacking [3–5]. The advantages of PV-membrane desalination technology are; (1) it utilises renewable solar energy, which significantly reduces reliance on fossil fuels and minimises greenhouse gas emissions associated with traditional desalination methods, thereby addressing environmental; (2) high economic viability even for small-scale applications in remote areas particularly in remote areas with high solar irradiance because PV systems offer low operational costs since solar energy is free and requires minimal maintenance [6,7]. PV-membrane desalination systems integrate solar energy with membrane filtration to produce clean water from brackish or saline water sources. In these systems, photovoltaic panels generate direct current (DC) electricity, which powers high-pressure pumps that force feedwater through selected semi-permeable membranes, effectively filtering out total dissolved solids (TDS), bringing the water close to the salinity level suitable for human consumption [3,8].

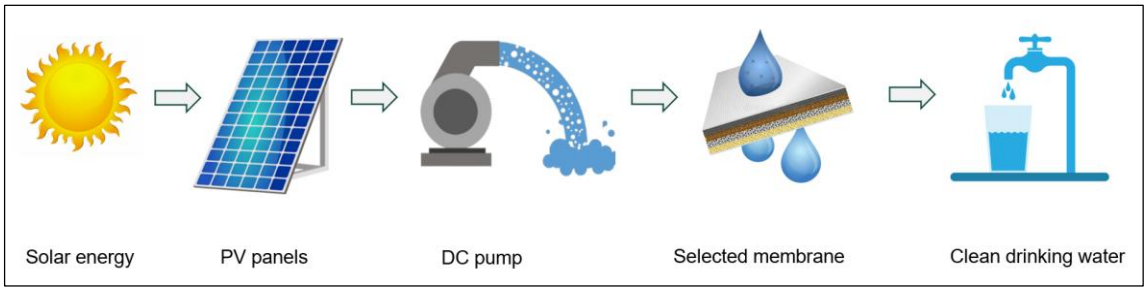


***Figure 1***. Illustration of the operation of the PV-membrane desalination system [*Source: Author's work*]

The performance of PV-membrane systems is however directly linked to solar irradiance (SI) availability, which fluctuates throughout the day and seasonally [9,10]. These variations in SI directly impact the performance of the PV-membrane system, leading to challenges in maintaining consistent water quality and production rates [9]. During periods of low SI, such as cloud cover or early morning/late afternoon hours, the decreased power output from PV panels can result in suboptimal membrane operating pressures [11–13]. This, in turn, may compromise permeate quality, reduce overall water production volume, and increase the specific energy consumption (SEC) of the desalination process [5]. To address the issue of SI fluctuations, researchers have explored various energy storage solutions, such as batteries and supercapacitors (SCs), to buffer against short-term and long-term SI fluctuation periods [14–16]. While these approaches have shown some efficacy, they also present limitations. In scenarios of prolonged low SI, storage capacities may become depleted without adequate opportunity for recharge, potentially leading to a complete system shutdown [14,15]. On the other hand, one effective solution to mitigate these challenges is the use of hydraulic buffering with pressure accumulators (bladder tanks) [17,18]. This method offers several advantages, including improved system resilience during periods of low SI by storing excess energy in the form of pressurised

water [19]. Thus, the bladder tank can maintain operational pressure within the system even when PV power decreases [19]. By integrating a hydraulic buffering system, this research aims to significantly improve the overall performance and reliability of the PV-powered membrane desalination system. Therefore, there is a critical need to develop advanced control methods that optimise the performance of PV-powered membrane desalination systems during SI fluctuations periods for continuous operations.

The development of advanced control methods for PV-membrane desalination systems represents a critical area of research with significant implications for improving water access in remote and off-grid communities. The adaptability of hydraulic buffering control methods to varying scales, from small community setups to larger agricultural applications, highlights their potential for widespread adoption in decentralised systems. By enhancing system resilience to SI fluctuations, it may be possible to achieve more consistent and efficient operation, ultimately increasing the reliability of these decentralised water treatment solutions. The applicability of this research extends beyond clean drinking water production. The ability to produce high-quality purified water in remote locations has important implications for advancing green hydrogen production technologies in Namibia. Electrolysis, a key process in hydrogen generation, requires ultrapure water as a feedstock. By providing a sustainable and reliable source of ultrapure water in off-grid areas, the PV-membrane system from this research project could contribute to the advancement of green hydrogen production technologies and support the transition to a hydrogen-based economy.

## 1.2. Statement of the Problem

The performance of PV-membrane desalination systems is negatively impacted by fluctuations in solar irradiance (SI) [9]. These fluctuations cause variations in system pressure, resulting in an inconsistent system operation, reducing the permeate quality and volume (production), and increasing the SEC during periods of low SI [9,10]. Current energy storage solutions have limitations in mitigating these effects, particularly during extended periods of low irradiance. Therefore, there is a critical need to develop advanced control methods to optimise the PV-membrane system performance under varying SI conditions to ensure consistent, efficient, and reliable operation.

## 1.3. Objectives of the Study

This research aimed to develop a hydraulic buffering control method to improve the performance of PV-membrane desalination systems during SI fluctuation periods. To achieve this, a hydraulic energy storage (bladder tank) was implemented and controlled to buffer periods of SI fluctuations. The specific objectives of this research were:

1. To design and simulate a photovoltaic-membrane system for optimal performance under varying SI conditions.
2. To conduct experiments and validate data to determine optimal operating PV-membrane conditions for continuous operation with a focus on PV power, system pressure, permeate quality, permeate volume (production), and specific energy consumption (SEC).
3. To develop a control algorithm for the optimal operation of the system incorporating a bladder tank as storage for buffering the system's operation during SI fluctuations.

## 2. LITERATURE REVIEW

In 2020, 2 billion people around the globe lacked access to safely managed drinking water, with 387 million people in Sub-Saharan Africa alone facing this problem, particularly in remote and off-grid areas [2]. To overcome this challenge, small-scale membrane systems powered by renewable technology such as PV were identified to provide an autonomous treatment option for remote areas, especially for those that are far from the electricity grid or have an unreliable grid connection [3–5]. PV-powered renewable energy (RE)-membrane systems are a promising solution in areas of high solar irradiance where brackish groundwater is the only available water source as these systems are energy-independent and cost-effective [5]. As discussed in **Section 1.1**, these systems work by using the power generated by the PV panels to drive a DC pump, which pumps brackish water through a selected membrane (ultrafiltration (UF)/nanofiltration (NF)/reverse osmosis (RO)) at high pressure, so that the TDS is filtered out, bringing the water close to the salinity level suitable for human consumption [4,5].

### 2.1. Effects of Solar Irradiance (SI) Fluctuations in PV-Powered Membrane Systems

While PV-powered membrane systems offer numerous advantages, such as environmental sustainability and reduced reliance on fossil fuels, their performance is significantly affected by fluctuations in solar irradiance (SI) [9,10]. These systems depend heavily on consistent solar energy to power the various components, especially pumps, which are critical for maintaining adequate pressure across the membranes. However, the intermittency of SI is a common challenge in solar-powered systems and can be attributed to several environmental factors, such as passing clouds, seasonal variations, and

fluctuations in ambient temperature [11–13]. As these factors lead to frequent and sometimes unpredictable changes in solar energy availability, the performance of the entire membrane system becomes highly variable.

Fluctuations in SI can directly impact several key performance metrics of PV-powered membrane systems, including the quality of permeate, the volume of permeate produced, SEC of the PV-membrane system, and the overall flow rate through the system [9,10]. For instance, during periods of low SI, less power is delivered to the pump, reducing its ability to push water through the membranes at the required high pressure, which in turn decreases the volume of permeate produced and reduces the flow rate [10]. This phenomenon was highlighted in a study by Boussouga et al. [10], where they observed a reduction in permeate production during low SI periods.

The relationship between SI and SEC is more complex. While lower flow rates during low SI periods suggest increased SEC, some studies have indicated that this is not always the case [13]. For example, research [13] has shown that averaging the power output over time, with periods of high SI compensating for those of low SI, can lead to more favourable SEC values. In addition to these effects, lower SI levels can also negatively impact the quality of the permeate [9]. When the power provided by the PV panels is not sufficient to maintain the required pressure across the membrane, the filtration process becomes less efficient. This can result in higher electrical conductivity (EC) in the permeate, indicating that the membrane is not adequately removing solutes from the feedwater [9]. In extreme cases, prolonged periods of low SI can cause the system to stop altogether, severely impacting its ability to operate at optimal performance.

## 2.2. Membrane Desalination Technologies

Membrane desalination systems utilise a range of membranes, each suited to specific operational needs based on their pore sizes and filtration capabilities [20–23]. UF membranes, with pore sizes ranging from 0.01 to 0.1 μm, are typically employed in pre-treatment stages to remove larger particles, such as suspended solids and bacteria, which helps protect more delicate membranes like NF and RO from fouling [22,23]. NF membranes, with pore sizes between 1-5 nm, are effective in filtering divalent ions, such as calcium and magnesium, and larger organic molecules, making them ideal for applications like water softening and brackish water desalination [21,23]. RO membranes, with pore sizes below 1 nm, provide the finest filtration, capable of removing monovalent ions like sodium chloride (NaCl), thus achieving high salt rejection rates essential in seawater desalination [20,22].

UF membranes are widely used as a pre-treatment before NF and RO membranes as they help reduce fouling by removing larger contaminants [23]. This improves the performance and extends the lifespan of the NF and RO membranes by decreasing the need for frequent cleaning and maintenance. In brackish water desalination, particularly in laboratory settings with salinity levels around 5 g/L, NF is often preferred over RO due to its lower operating pressure and energy requirements while still providing effective salt rejection [20,21,23]. This makes NF a more energy-efficient solution for moderate salinity levels, whereas RO, though more effective for higher salinity, requires greater pressure and energy.

Other membrane processes such as pervaporation (PV), electrodialysis (ED), membrane distillation (MD), and membrane crystallization (MCr) also play significant roles in desalination, though they are less commonly used than NF and RO [21]. PV separates liquids by evaporating volatile components through a dense membrane, making it suitable for certain desalination applications. ED, on the other hand, separates ions using an electric potential, which is especially useful for treating low-salinity brackish water. MD utilises a temperature gradient to drive water vapour through a hydrophobic membrane, retaining non-volatile salts, while MCr focuses on recovering minerals during desalination by combining MD with crystallisation.

### 2.3. Effects of Pressure Fluctuations in PV-Powered Membrane Systems

Membranes are expected to operate at constant operating conditions without abrupt pressure or crossflow variations to maintain steady and optimal system performance [9]. Variability in power supply to the pump due to SI fluctuations can cause pressure fluctuations in the system, which reduces the overall system performance, such as reduction in flux and permeate quality [9,13]. In NF and RO membranes, both representing the common membranes used in membrane-based water desalination systems, abrupt pressure or flow fluctuations can result in decreased flux and permeate quality [24,25]. Reduction in pressure directly reduces the permeate flux through the membrane, while the reduction in cross-flow velocity induces the build-up of retained salts on the membrane surface, which results in an increased salt diffusion across the membrane, thus decreasing the permeate quality [26]. In addition, pressure fluctuations in such systems can result in decreased SEC of the system [10,27].

## 2.4. Methods of Regulating Pressure Fluctuations in PV-Membrane Systems

Several strategies of control have been implemented in membrane systems to regulate pressure fluctuations caused by SI fluctuations [14–18,28–35]. These methods of control include energy buffering solutions such as the use of batteries, supercapacitors (SCs), and pressure vessels.

### 2.4.1. Energy Buffering with Supercapacitors and Batteries

Existing approaches to mitigating the impact of SI fluctuations on PV-powered membrane systems were investigated with a focus on electrical energy storage solutions, such as batteries and SCs [14]. These storage solutions were used to buffer excess energy during low SI periods and provide backup power during low irradiance conditions [14,15]. SCs were used in PV-powered membrane systems for short-term energy buffering [16,28]. SCs have proven to be good candidates for short-term energy buffering due to their ability to persist hundreds of thousands of charge/discharge cycles, ability to provide large amounts of instantaneous power, high energy storage efficiency (85-98%) and longer lifetime (8-12 years) than batteries [16,28,29]. Although SCs pose numerous advantages, the amount of electrical energy that can be stored in them is limited, typically providing energy buffering for a period of few minutes [16]. In addition, SCs have a high self-discharging rate, calculated to be 1.5% per day [15].

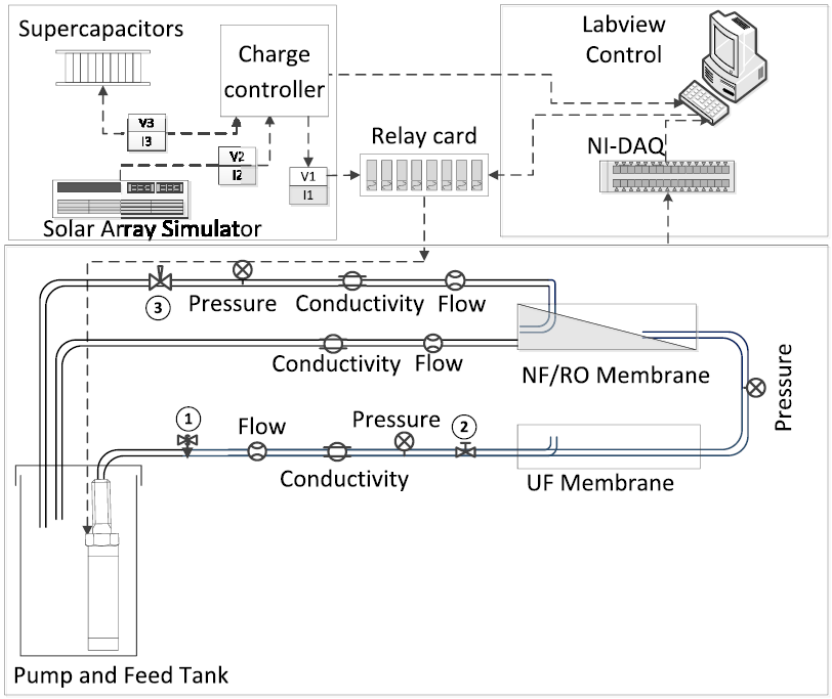


***Figure 2***. Electrical energy buffering control incorporating a supercapacitor [15]

Batteries are widely employed in PV-membrane systems for long-term energy buffering, enabling continuous and stable performance during low SI conditions [30]. Lead-acid (LA) batteries in particular, were deployed in PV-membrane systems due to their relatively low cost compared to Li-ion batteries and global availability [31]. However, LA batteries have low efficiency (75-84%), have limited number of charging/discharging cycles (~2000), low depth of discharge (DoD) less than 50%, and low lifetime (3-5 years) [31,32]. An alternative to LA batteries are Li-ion batteries, which are currently favoured in transportation system applications due to their long lifetimes (10 years), increased number of charging/discharging cycles (~4000), higher efficiency (>90%), and higher DoD (>80%) [33]. However, Li-ion batteries remain more expensive compared to LA batteries [34].

### 2.4.2. Energy Buffering with Hydraulic Energy Storage (Pressure Accumulator)

An alternative to the use of electrical energy storage for buffering control is hydraulic energy storage, where pressure accumulators have been used as a mechanical alternative in PV and wind membrane desalination systems to buffer energy for short-term periods [17,18]. Pressure accumulators are essential components in hydraulic systems, particularly in applications requiring energy buffering, such as PV-powered membrane desalination systems [36]. They store energy as pressurised fluid, enabling stable operation during fluctuations in energy supply [19].

Various types of pressure accumulators exist, including bladder tanks, diaphragm tanks, piston accumulators, and spring accumulators. Bladder tanks, which consist of an elastic bladder within a rigid outer shell, are the most common. They operate by expanding and contracting as fluid enters and exits, thus maintaining pressure [19]. Diaphragm tanks function similarly but utilise a diaphragm to separate the gas and liquid, offering a more compact design [19]. Piston accumulators employ a piston to provide high pressure and capacity but can be bulkier [37]. Spring accumulators are less common due to their limited capacity [36]. The operation modes of pressure accumulators include charging and discharging. In charging mode, fluid fills the accumulator, compressing the gas or bladder; during discharging, the stored fluid is released to maintain system pressure during demand spikes [19]. The advantages of pressure accumulators include rapid response times to pressure changes and minimal maintenance compared to electrical storage systems. However, they also have disadvantages such as limited storage capacity and potential wear over time [19]. Bladder tanks are often preferred due to their efficiency in maintaining

pressure and their compact design. They require less maintenance than piston accumulators and can be easily integrated into existing systems, making them ideal for renewable energy applications where reliability is crucial [19].

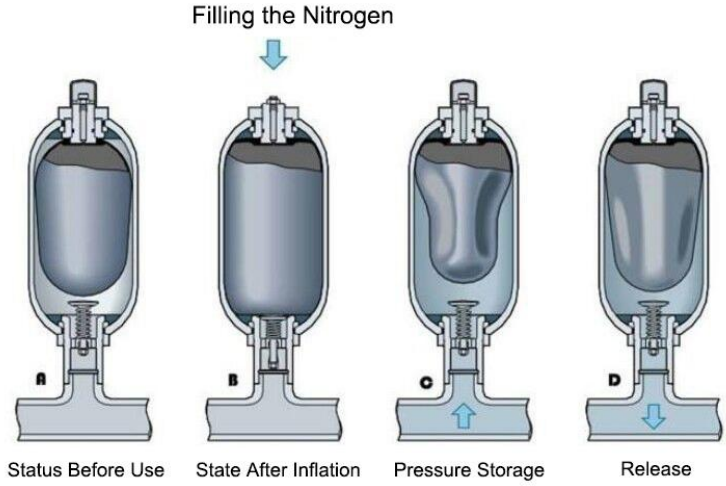


***Figure 3***. Illustration of the charging and discharging of a bladder tank [38]

Karavas et al. [17] investigated a PV-powered small-scale seawater reverse osmosis (SWRO) desalination system that employed bladder pressure tanks in hybrid with capacitors for short-term energy buffering. The capacitors allowed the system to operate for 10 minutes during low SI periods until the pump shut down due to the lack of power when the capacitors were discharged, after which the bladder pressure tanks enabled the system to operate again with pressurised feed seawater for a further 20 minutes. In a separate study, Liu *et al*. [18] developed a feedback control algorithm for a wind-powered reverse osmosis desalination system for brackish water desalination to regulate the feed pressure and flowrate based on the available pressure in a hydraulic accumulator (300 L) and a series of solenoid valves. The control algorithm enabled the system to be operated under low wind speeds of about 4 m/s with a 97% average salt retention. Both control

algorithms allowed for continuous operation of the desalination systems while also achieving higher efficiencies and lower specific energy consumption (SEC). Although pressure accumulators are viable in RE-membrane desalination systems, they have been shown to be cost-effective only for larger systems [35]. Additionally, advanced energy management and control of high temporal resolution are required.

Given the limitations of traditional electrical energy storage solutions, there is a need to develop advanced control methods to optimise the performance of PV-powered membrane systems during continuous operations under varying SI conditions while relying on pressure accumulators as energy storage.

# 3. RESEARCH METHODOLOGY

## 3.1. Research Design

The research methodology employed in this study is designed to address the challenges posed by SI fluctuations on the performance of PV-membrane systems for water purification. It begins with a comprehensive research design that outlines the system's operational principles and components, followed by detailed data collection methods to ensure a thorough understanding of each part's contribution to functionality.

Key phases of the experimental design include conducting steady-state threshold tests to establish baseline performance metrics and passive and uncontrolled buffering experiments to evaluate system behaviour under varying SI conditions. An important aspect of the methodology is the development of a control algorithm that controls the hydraulic bladder accumulator, allowing it to discharge during low SI periods and charge during high SI periods by monitoring power ramp-down rates.

Data analysis is systematically performed to interpret results, focusing on metrics such as permeate quality, permeate volume (production), and SEC. This methodology effectively integrates theoretical frameworks with practical experimentation, providing insights into enhancing the reliability and efficiency of PV-powered membrane systems.

3.2. Experimental Setup and Data Collection

3.2.1. System Design Layout and Operational Principle

The schematic of the experimental setup is shown in **Figure 4** and a snapshot of the laboratory installation of the actual PV-membrane system is shown in **Figure 5**.

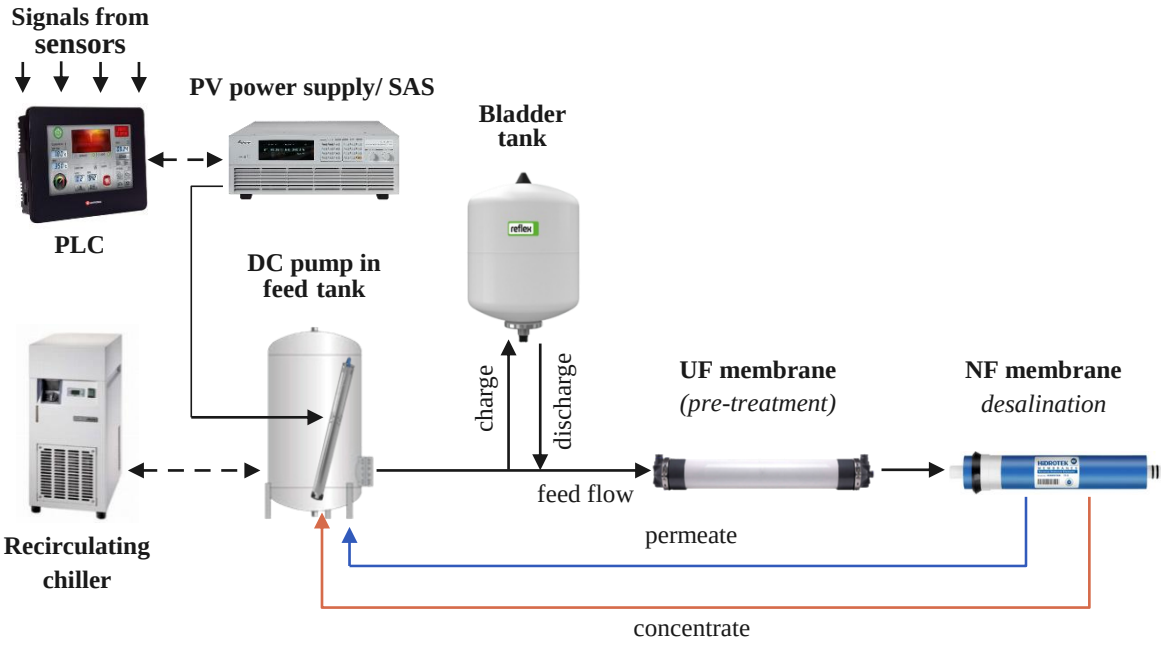


***Figure 4.*** PV-membrane system equipped with a hydraulic bladder tank for pressure buffering [*Source: Author's work*].

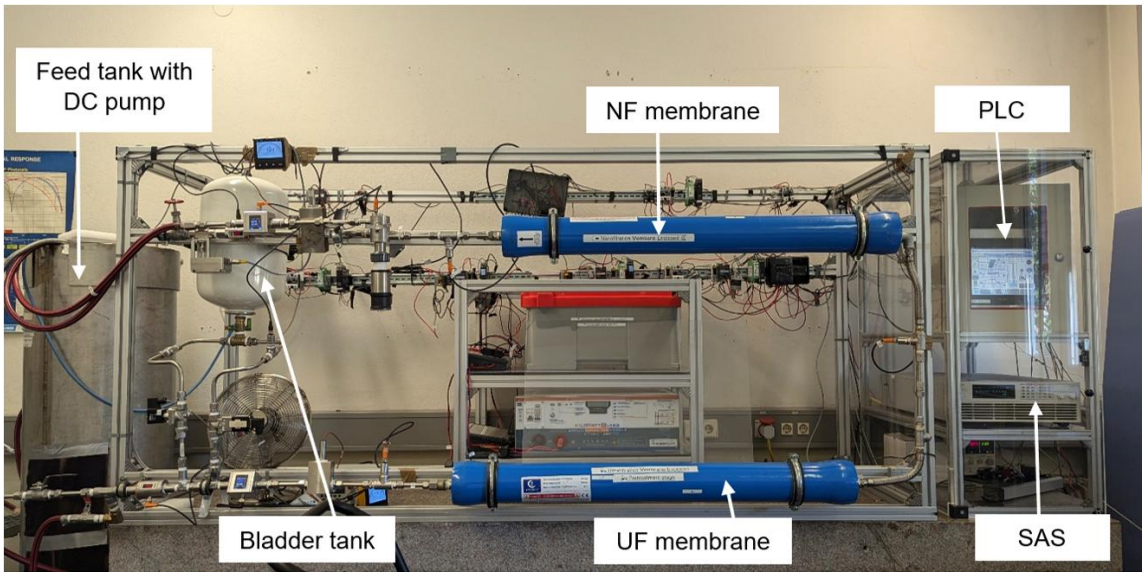


***Figure 5***. System setup in the laboratory [*Source: Author's work*].

The operational principle of the photovoltaic-powered membrane (PV-membrane) system was designed to facilitate efficient water filtration through a combination of ultrafiltration (UF) and nanofiltration (NF) processes. As shown in **Figure 4** and **Figure 5**, the system utilized the Inge Dizzer P 4040-6.0 UF membrane for pretreatment, followed by the FilmTech NF90-4040 membrane for desalination. A solar array simulator (SAS: Chroma 62000H) was employed to simulate and replicate various solar irradiance intensities and temperatures of the PV panels (OffGridTec PCB-ETFE Semi-flexible) based on data recorded from the Karlsruhe Institute of Technology (KIT) solar park in Germany. This approach ensured the reproducibility of the experiments by using real-world measured solar irradiance and temperature in an indoor laboratory setting.

The power generated by the SAS was utilised to drive a DC pump (Grundfos SQF 0.6 - 2 N), which was employed to achieve the desired system flow rate and pressure. The pump

was equipped with a maximum power point tracker (MPPT) designed to extract the maximum available power from the PV panels.

The pump was submerged in a 180 L feed tank containing synthetic brackish water with a salt concentration of 5 g/L (9.23 mS/cm). A recirculating chiller (LAUDA LWG 160 Model WKL 903) was connected to the feed tank to maintain a constant feed water temperature within a range of 19 °C to 21 °C. Furthermore, a 25 L hydraulic bladder tank (Reflex Refix DD 25), with a maximum useful capacity of 18.7 L, was integrated into the system to buffer feed pressure during periods of low solar irradiance.

The system was equipped with various sensors and meters, including pressure sensors, flow meters, voltage sensors, current sensors, electrical conductivity (EC) sensors, and temperature sensors. Current (Phoenix Contact MCR-S-1-5-UI-DCI) and voltage (Omega Uni-/Bipolar DRST-CM 300 VDC) sensors were installed to measure the electrical characteristics of the pump. Inline pressure (Burkert 8316) sensors, flow meters (iFM SM600 and KOBOLD MIM-1205HG4C3TO), and EC sensors (Burkert 8222) were used to measure pressure, flow rate, and EC in the feed, permeate, and concentrate streams of the PV-membrane system to monitor instantaneous performance.

All sensor data was transmitted to a programmable logic controller (PLC: Unitronics Unistream 10.4”), which incorporated a control algorithm designed to manage the charge and discharge cycles of the hydraulic bladder tank in response to fluctuations in solar irradiance. This algorithm played a crucial role in maintaining system stability and

performance under varying solar irradiance conditions, thereby enhancing the reliability of the PV-membrane system for continuous water purification.

### 3.2.2. System Components Description

The components outlined below were used to build a laboratory-based PV-powered membrane desalination prototype:

**a. Solar Array Simulator (SAS)**

***Figure 6.*** Chroma Programmable DC Power Supply (with Solar Array Simulation) [39]

**<u>Model/Specifications</u>**

- Model 62000H (62050H-600S) Series
- Output Voltage: 0 to 600 V
- Output Current: 0 to 8.5 A
- Output Power: 5000 W

This DC power source acts as a controllable (programmable) solar array simulator [39]. The Chroma 62000H Series offers programmability for precise control of voltage and

current output, enabling users to replicate various solar irradiance intensities and analyse membrane performance under different weather conditions scenarios. Additionally, it can generate critical I-V (current-voltage) curves, providing valuable insights into the electrical behaviour of the membranes under simulated SI conditions.

**b. Ultrafiltration (UF) Membrane**

***Figure 7.*** Dizzer P UF Membrane [40]

**Model/Specifications**

- Inge VK-0049 Dizzer P 4040-6.0 Ultrafiltration Module
- Max Pressure: 3.0 bar (43.5 psi)
- Max Temperature: 41.4 °C (104 °F)
- Membrane Active Area: 6.0 $m^2$ (65 $ft^2$)

UF membranes are used as a pre-treatment for NF/RO to prevent them from fouling and increase their life expectancy. They play a vital role in protecting and enhancing NF/RO performance. The Inge VK-0049 Dizzer P 4040-6.0 Ultrafiltration (UF) Module acts as a vital pre-filter within the PV-membrane system [40]. This component uses hollow fibre membranes containing pores typically sized between 0.01-0.1 μm. These pores allow

water molecules to pass through while rejecting and concentrating larger contaminants in a separate retentate stream. The UF membrane functions through a pressure-driven process where pressurised feedwater flows through the hollow fibres, achieving purification. It removes impurities like colloids, microorganisms, and organic substances from the raw feedwater. This pretreatment step safeguards the integrity and performance of downstream membranes within the PV system by preventing potential fouling.

### c. Nanofiltration (NF) Membrane

***Figure 8***. FilmTec™ NF Membrane [41]

**Model/Specifications**

- FilmTec™ NF90-4040 Membrane
- Membrane Type: Polyamide Thin-Film Composite
- Maximum Operating Pressure: 41 bar (600psi)
- Maximum Operating Temperature: 45°C (113°F)
- Permeate Flow Rate: 7.6 $m^3$/d (2000 gpd)
- Minimum Salt Rejection: 98.7%

The NF90-4040 membrane is a key component for filtration in a PV-membrane system. It utilises a polyamide thin-film composite structure [41]. The NF90's dense layer is specifically designed to allow some single-charged ions (monovalent ions) to pass through while rejecting larger molecules and ions with multiple charges (multivalent ions). Unlike UF membranes, it filtrates based on size and charge. The pressure-driven NF process removes targeted contaminants like pesticides and certain salts, optimising downstream membrane performance. The NF90-4040's design and process enable selective pre-treatment within PV-membrane systems.

**d. Pressure Sensor**


***Figure 9***. Burkert Pressure Sensor [42]

**<u>Model/Specifications</u>**

- Burkert Pressure Measuring Device: Type 8316
- Output signal: $P_{max}$: ≤ 0.6 bar: standard signal 4 to 20 mA (two-wire)

  $P_{max}$: > 0.6 bar and ≤ 60 bar: standard signal 4 to 20 mA (two-wire) or 0 to 10V DC (three-wire).

$P_{max}$ = 100 bar; standard signal 4 to 20 mA (two-wire)

- Load: $P_{max}$: ≤ 0.6 bar: < (U - 10 V) / 0.02 A (in Ω)

  $P_{max}$: > 0.6 bar: < (U - 7 V) / 0.02 A (in Ω)

- Current consumption Max.: 23 mA
- Insulation voltage: 500 V DC
- Medium fluid temperature

Pressure sensors are used for pressure measurement of water in both the feed and concentrate streams in the PV-membrane system [43]. They have a sensing element of constant area, which reacts to the force applied by the water pressure. The sensing element must respond fast enough to notify the operators or initiate automatic safety actions during transient states, such as abrupt pressure changes. The Burkert Type 8316 pressure sensor ensures the safe, efficient, and optimised operation of PV-membrane systems. The pressure data collected by the pressure sensor is important for three main reasons: it safeguards the system by allowing for real-time monitoring and intervention to prevent pressure from exceeding safe limits and potentially damaging membranes or other components. Additionally, pressure data is important for optimising processes within the system, such as regulating feed flow rates or ensuring optimal membrane performance.

**e. Flow Meter/Sensor**

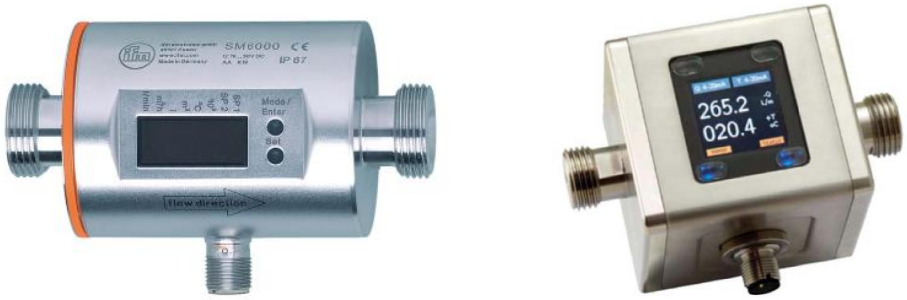


***Figure 10***. iFm Magnetic-inductive Flow Sensor and KOBOLD Magnetic-inductive Flow meter [44,45]

**Model/Specifications**

iFm Magnetic-inductive Flow Sensor:

- Type: SM6000
- SMR12GGXFRKG/US-100
- Number of inputs & outputs: number of digital outputs: 2; number of analogue outputs: 1
- Measuring range: 0.1 to 25 L/min (0.005 to 1.5 $m^3/h$)
- Medium temperature: -10 to 70 °C
- Compressive strength: 16 bar
- Operating voltage: 18 to 30V DC

KOBOLD Magnetic Inductive Flowmeter:

- Model: MIM-1205HG4C3TO
- Measuring range: 0.01 to 1 L/min, 1.5 to 650 L/min
- Maximum pressure: 16 bar
- Maximum temperature: 140 °C

- Material: stainless steel, PEEK

Flow meters/sensors are employed within PV-membrane systems to measure the volumetric flow rate of conductive liquids. Flow meters measure the flow rates of the water (feed, permeate, concentrate) in the PV-membrane system. For the SM6000 and MIM, Faraday's Law of electromagnetic induction governs their operation [44,45]. As conductive fluid flows through a magnetic field generated by the sensor, a voltage is induced between electrodes within the sensor. This voltage is directly proportional to the fluid's velocity. The flow meter then converts this voltage into a measurable electrical signal that reflects the flow rate. They are more susceptible to failure than other sensors as they often contain moving parts. They allow fluid flow monitoring, control, and optimisation.

**f. Electrical Conductivity (EC) Sensor/Meter**

***Figure 11***. Burkert Conductivity Meter [46]

**Model/Specifications**

- Burkert Conductivity Meter: Type 8222
- Conductivity measurement range: 0.05 µS/cm to 10 mS/cm
- Temperature measurement range: - 20 to 100 °C (- 4 to 212 °F)

The Burkert Type 8222 conductivity meter measures the electrical conductivity of liquids in PV-membrane systems [46]. EC sensors measure the electrical conductivity of the feed, concentrate and permeate, which is determined by using the distance between the electrodes with a known surface area. The data collected by the EC sensor is important for monitoring feedwater and permeate quality, evaluating membrane performance, and optimising processes like cleaning cycles. The Type 8222 conductivity meter plays a big role in maintaining a well-functioning PV-membrane system by ensuring optimal water quality and efficient membrane function.

g. Current Transducers

***Figure 12***. Phoenix Current Transducer [47]

**Model/Specifications**

- Phoenix Contact MCR-S-1-5-UI-DCI
- Supply voltage range: 20 V DC to 30 V DC
- Current consumption maximum: < 40 mA (no load)
- Input current range: 0 to 11 A AC/DC (permissible permanent overload: 120 %)
- Number of inputs: 3

The Phoenix Contact MCR-S-1-5-UI-DCI is a programmable current transducer specifically designed to measure various current types in industrial settings [47]. The device functions by converting a wide range of DC, AC, and distorted currents (with harmonics) within a specified input range (0 A to 11 A) into a proportional output signal. The MCR-S-1-5-UI-DCI current transducer offers programmability and configurability, allowing users to tailor its measurement range and output characteristics to their specific needs. In PV-membrane systems, it plays a crucial role by accurately monitoring and transmitting real-time current data from various sources, such as the output of the PV membranes themselves or the current flowing through the pump and other electrical components. This data is essential for performance monitoring, troubleshooting potential issues, and optimising the overall efficiency of the PV-membrane system.

### h. DC Voltage Transmitters


***Figure 13***. Omega Engineering DC Signal Transmitter [48]

**Model/Specifications**

- Omega Engineering, Universal Uni-/Bipolar DC Signal Transmitter
- DRST-CM 300 VDC
- Universally Powered by 21.6-253 VAC / 19.2-300 VDC
- Max. Required Power: 2.5 W
- Operating Temperature: -20 to 60°C
- Relative Humidity: < 95% RH (non-cond.)

This is a universal uni-/bipolar DC signal transmitter designed for versatile voltage measurement applications [48]. This device accepts a wide range of DC voltage inputs (from millivolts to 300 VDC) and converts them into a proportional standard output signal, typically 4 - 20 mA or 0 -10 V. The DRST-CM boasts high accuracy (0.05%) and configurability, allowing users to tailor its input and output ranges to precisely match the specific voltage measurements required. In PV-membrane systems, the DC voltage transmitter monitors and transmits real-time voltage data from various sources, such as

the output voltage of the PV membranes themselves or the voltage across control elements within the system. This accurate voltage data is crucial for performance evaluation, fault detection, and optimising the overall efficiency of the PV-membrane system.

### i. Recirculating Chiller

***Figure 14***. LAUDA LWG Recirculating Chiller [49]

**Model/Specifications**

- LAUDA LWG 160 Model WKL 903 Recirculating Chiller
- Working Temp Range: -15 to 40°C
- Filling Volume: 8 to 12 L
- Electrical Voltage & Frequency: 230 V/50 Hz
- Cooling Design: Air-Cooled
- Maximum Pump Pressure: 3.2 bar
- Maximum Pump Flow: 33 L/min
- Cooling Output at 20 °C: 0.80 kW

The LAUDA® LWG 160 Model WKL 903 Recirculating Chiller is a vital component in PV-powered membrane desalination systems, operating within a temperature range of -15 to 40°C with a cooling output of 0.8 kW at 20°C and a maximum flow rate of 33 L/min [49]. This air-cooled chiller ensures optimal feed water temperatures, preventing overheating that could damage membranes, while its energy-efficient design allows it to be powered by solar energy, reducing operational costs. Its robust construction supports continuous operation, which is essential for maintaining efficiency in desalination processes, and it can integrate with smart monitoring systems for optimised control based on solar generation patterns.

**j. Safety Valve**

***Figure 15***. Goetze Safety Valve [50]

**Model/Specifications**

- Goetze Series 460 Safety Valve
- Operating temperature range: -60 to 225 °C

- Operating pressure range: 0.2 to 25 bar
- Size: DN 10 to DN 25, 3/8" to 1"
- Material: Stainless Steel

In PV-membrane systems, a safety valve acts as a pressure relief mechanism [50]. It is a spring-loaded device installed within the piping or enclosure of the system. During abnormal operating conditions, such as excessive pressure buildup due to thermal expansion, pump malfunctions, or gas generation, the safety valve opens. This controlled release of pressure prevents damage to the membranes and other system components by ensuring pressures remain within safe operating limits. These valves are crucial for safeguarding system integrity and ensuring the safe operation of PV membrane systems.

**k. Normally Closed (NC) Solenoid Valve**


***Figure 16***. End Armaturen NC Solenoid Valve [51]

**<u>Model/Specifications</u>**

- End Armaturen (EA) 2/2-solenoid valve,
- Model: MEMG2Z322245015/C
- Voltage: 24V DC
- Size: 1/2"
- Body material: Stainless Steel
- Function: Combined operated – NC
- Seals material: NBR
- Nominal pressure min.: 0 bar
- Nominal pressure max.: 10 bar
- Temperature range min.: 0 °C
- Temperature range max.: +35 °C

The End Armaturen (EA) 2/2-solenoid valve is an electromechanical device equipped with a plunger that remains closed until it receives an electrical impulse [51]. When energised, the magnetic field generated overcomes the attractive force of permanent magnets, causing the valve to open and release pressure. In the PV-membrane desalination system, this device is essential as it is controlled to charge and discharge the bladder tank during SI fluctuations.

**l. Pressure Accumulator (Bladder Tank)**


***Figure 17***. Reflex Refix Pressure Accumulator [52]

**Model/Specifications**

- Reflex Refix DD 25
- Type: DD 25
- Nominal volume: 25 L
- Max. useful volume: 18.7 L
- Max. permissible system temperature: 70 °C
- Min. perm. operating temperature: -10 °C
- Max. perm. operating temperature: 70 °C
- Max. perm. operating pressure: 10 bar
- Factory-provided gas supply pressure: 4 bar

The Reflex Refix DD 25 pressure accumulator functions as a pressure stabilization and energy storage device [53]. It consists of a pressure vessel containing a gas-preloaded bladder or diaphragm that separates the pressurised hydraulic fluid from the inert gas (nitrogen). Its design allows for efficient balancing of pressure without the need for

electrical power. During periods of high system demand, the accumulator releases stored hydraulic water, supplementing the pump and maintaining consistent system pressure. Conversely, when pressure surges due to sudden flow fluctuations, the accumulator absorbs excess water, acting as a pressure dampener and mitigating shock. This pressure buffering mechanism safeguards system components from excessive pressure spikes and optimises pump operation by reducing pressure fluctuations and minimising energy consumption.

### m. Programmable Logic Controller (PLC)


***Figure 18***. Unitronics Unistream PLC [54]

**Model/Specifications**

- Unitronics Unistream, 10.4"
- Input voltage: 12 VDC or 24 VDC
- Permissible range: 10.2VDC to 28.8 VDC
- Maximum current consumption: 1.62 A at 12 VDC, 0.81 A at 24 VDC
- Processor: 32 bit, 800MHz RISC Processor, with Graphic Accelerator

The Unitronics Unistream, 10.4" A PLC acts as the brains of an industrial automation system [54]. This modular system allows users to customise their setup by selecting the necessary I/O modules, which can be mounted directly onto the back of the HMI or on a DIN rail, facilitating flexibility and cost efficiency. It is programmed to make decisions based on real-time data. In a PV-membrane system, it receives data from sensors and switches, interprets it using the control algorithm, and then controls devices like pumps and valves, to influence the physical process. This allows for the automation of complex tasks of the PV-powered membrane system.

**n. Photovoltaic (PV) Panels**

***Figure 19***. OffGridTec PCB-ETFE PV Panels [55]

**Model/Specifications**

- OffGridTec PCB-ETFE 100W 39,6V Semi-flexible Solar panel

- Working voltage (Vmp): 39,6 V
- Open circuit voltage (Voc): 46.61 V
- Maximum current (Imp): 2,53 A
- Short circuit current (Isc): 2,73 A
- Solar cells material: monocrystalline A-grade solar cells

The OffGridTec PCB-ETFE Semi-flexible solar panels consist of an array of solar cells, fabricated from semiconducting materials like silicon [55]. The ETFE (ethylene tetrafluoroethylene) coating enhances durability and resistance to environmental factors, ensuring long-term performance even in harsh conditions. The system comprised of 6 PV modules connected in a 3 series x2 parallel configuration. This configuration achieves a maximum power output of 600 W, a maximum voltage of 118.80 V, and a maximum current of 5.06 A.

**o. Direct Current (DC) Pump**

***Figure 20***. Grundfos DC Pump [56]

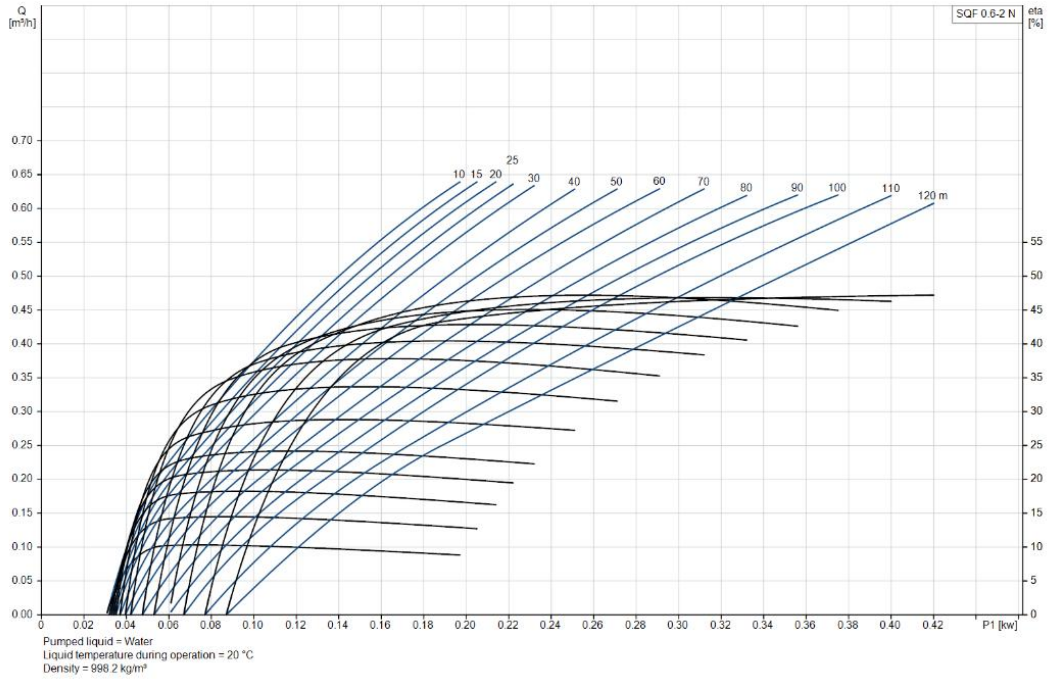


***Figure 21***. Grundfos DC pump performance curve [56]

## Model/Specifications

- Grundfos SQF 0.6 - 2 N Pump
- Maximum ambient pressure: 15 bar
- Maximum operating pressure: 15 bar
- Pump material: Stainless steel
- Pumped liquid: Water
- Liquid temperature range: 0 to 40 °C
- Selected liquid temperature: 20 °C
- Density: 998.2 kg/m³
- Power input - P1: 1.4 kW

- Rated power - P2: 1 kW
- Rated voltage AC: 1 x 90-240 V
- Rated voltage (DC) and current: 30-300 VDC, 8.4 A
- Rated speed: 3600 rpm

A pump is one of the key components of the PV-membrane system as it produces the feed flow rate and pressure required for the membranes and defines the power requirements from the PV panels. The Grundfos SQF 0.6-2 N pump is for fluid circulation and pressurisation in PV-membrane systems [56]. Its helical rotor design tackles high-pressure requirements. A major advantage is its dual power source compatibility (AC or DC). This allows direct operation from the system's DC solar panels. Within the system, the SQF 0.6-2 N circulates feedwater, maintains pressure (if supplied with constant power), and even assists with membrane cleaning processes.

**p. Temperature Sensor Transmitter**


***Figure 22***. Uxcell Temperature Sensor Transmitter [57]

**Model/Specifications**

- Uxcell PT100 Temperature Sensor Transmitter
- Input voltage: 24 DC
- Measuring range: 0 to 100 °C
- Output current: 4 to 20 mA
- Measurement precision: ±0.2% FS

The Uxcell PT100 temperature sensor transmitter is a compact sensor that monitors the temperature of the feedwater in the feed tank of the PV-membrane system [57]. It utilises a Pt100 RTD that changes resistance with temperature. The transmitter converts this change into a standard signal for easy integration into the system's data network. Accurate temperature control is important in PV-membrane systems as it ensures optimal membrane performance and prevents damage from excessive heat. Moreover, temperature data from the sensor is crucial for system optimization.

### 3.3. System Simulation

Prior to control algorithm development, simulations were conducted using MATLAB Simulink to evaluate the PV-membrane desalination system's performance under varying solar irradiance (SI) conditions. The simulation modelled system dynamics, including hydraulic buffering, with key parameters such as PV power output, feed pressure, bladder tank charge and discharge, and permeate flow rates. Real-world SI profiles data recorded from the KIT solar park in Germany were used to replicate cloudy conditions. Performance metrics such as SEC, water recovery, and permeate quality were calculated, and sensitivity analyses assessed the impact of input variability on system stability. The

simulation provided insights that guided experimental design decisions, demonstrating the potential of hydraulic buffering to mitigate performance instability.

## 3.4. Experimental Design

To develop a control algorithm for buffering the PV-membrane system feed pressure, an experimental design was created where filtration experiments were conducted in four phases; steady-state threshold tests, passive (directly-coupled) experiments, uncontrolled buffering experiments, and controlled buffering experiments. An NF90-4040 membrane was selected and used for desalination because of its lower operating pressure and energy requirements while still providing effective salt rejection which makes it a more energy-efficient solution for moderate salinity levels such as 5g/L used in this system. The feedwater used for experiments was prepared in the laboratory using NaCl and deionized water to create synthetic brackish water with a salt concentration of 5 g/L (9.23 mS/cm).

### 3.4.1. Steady-state threshold tests

Steady-state threshold tests were performed to determine the minimum operating pressure ($P_{min}$) and the optimal setpoint pressure ($P_{set}$) for the PV-membrane system. The tests were conducted at different feed pressure levels: 2, 3, 4, 5, 6, 7, 8, 9, 10, 11, and 12 bar. During the tests, data, including maximum pump power consumed, flow rate, SEC, flux, EC, salt rejection, and water recovery, were recorded. The obtained data was analysed where $P_{min}$ and $P_{set}$ were identified. The optimal setpoint pressure was then used as the operating feed pressure for all experiments (passive, uncontrolled buffering, and controlled buffering). Throughout these tests, the SAS supplied a consistent voltage of

118.8V and a current of 5.06A, representing the maximum voltage and current output achievable from the PV panels. These voltage and current values were maintained by the SAS throughout all steady-state tests conducted at varying feed pressure levels.

### 3.4.2. Passive (Directly-coupled) Experiments

During the second phase of the experimental design, passive experiments were carried out to analyse the system's performance without pressure buffering (hydraulic bladder tank shut off). The energy consumption and pump utilisation were studied, along with the system's efficiency and conversion losses. Furthermore, the pump shutdown pressure in relation to SI fluctuations was determined and later used for the development of the control algorithm.

The experiments were conducted over three solar days with varying SI conditions (sunny, partly cloudy, very cloudy). The SI data were selected to represent different levels of SI fluctuations that occurred within 1 year of data namely: sunny day (5 May 2016), partly cloudy day (26 May 2016), and very cloudy day (13 October 2016). The solar days' SI data with a resolution of 1 second (1-s) were collected via an irradiance sensor from the KIT solar park in Karlsruhe, Germany. The SI data was used as input for the SAS where it was converted into current-voltage (I-V) curves. Additionally, the temperature of the PV modules was recorded using an external temperature sensor, which was also used as input for the SAS.

### 3.4.3. Uncontrolled Buffering Experiments

The uncontrolled buffering experiments were conducted similarly to the passive experiments. However, in this scenario, the hydraulic bladder tank was left open instead of being shut, allowing it to charge and discharge throughout all three experiments of different SI fluctuation days (sunny, partly cloudy, and very cloudy). This was done to assess the bladder tank's ability to stabilise system feed pressure when uncontrolled during SI fluctuations. The data collected was analysed and later used for control algorithm development.

### 3.4.4. Control Algorithm Development and Controlled Buffering Experiments

Based on the results obtained from steady-state tests, as well as passive and uncontrolled buffering experiments, a control algorithm was developed. This algorithm allows the hydraulic bladder tank to charge automatically and discharge based on pressure fluctuations in the system. The charging and discharging of the bladder tank were controlled by normally closed valves (NC: End Amaturen 2/2-solenoid valves) which receive input signals from the PLC. The control algorithm was implemented in the Unitronics software which was uploaded onto the PLC.

Controlled buffering experiments were conducted in a similar manner to uncontrolled buffering experiments. However, in this case, the hydraulic bladder tank was first pre-charged to 12 bar and left shut before each of the three experiments (sunny, partly cloudy and very cloudy) began. This was done to assess the bladder tank's ability to stabilize system feed pressure and prevent system shutdown when the feed pressure is too low

during SI fluctuations. Furthermore, the data collected was used to improve the control algorithm.

**Table 1** presents a summary of the experimental design that was explained in detail in **Section 3.3**.

***Table 1.*** Summary of experimental design

| **Experiment** | **Conditions** | **Performance Analysis** | **Solar days** | **Membrane** |
|---|---|---|---|---|
| Steady-state threshold tests | Feed pressure varied from 2, 3, 4,…, 12 bar | Identify $P_{min}$ and $P_{set}$ | Constant output voltage (118.8V) and current (5.06A) | NF90-4040 |
| Passive (directly-coupled) | $P_{set}$ | Investigate pump energy consumption, utilisation, system efficiency, and conversion losses. Determination of shutdown pressure with respect SI fluctuations. | Sunny<br>Partly cloudy<br>Very cloudy | NF90-4040 |
| Uncontrolled buffering | $P_{set}$ | | Sunny<br>Partly cloudy<br>Very cloudy | NF90-4040 |
| Controlled buffering | $P_{set}$ | System performance analysis. | Sunny<br>Partly cloudy<br>Very cloudy | NF90-4040 |

| | | | | |
|---|---|---|---|---|
| | | Shutdowns and resilience analysis. | | |

3.5. Data Analysis

The data was analysed using OriginPro 2023b software. This software was instrumental in processing and visualizing the experimental data. The data was smoothed to reduce noise and random fluctuations in a dataset to have smoother data that can be visualised more clearly and easily. Additionally, OriginPro 2023b was used to create detailed graphs that illustrated the relationships between key variables, such as PV power, SEC, pressure, flow rate, flux, production, EC, rejection, and recovery. These graphs helped in identifying trends, patterns, and correlations within the data.


***Figure 23***. OriginPro 2023b software [58].

The data analysis incorporated a detailed uncertainty evaluation to ensure the reliability and accuracy of both experimental and numerical results. Instrumentation uncertainty was addressed by calibrating all measurement devices, with error margins provided by manufacturers, such as ±0.5% FS for pressure sensors and ±1% FS for flow meters.

Repeatability was assessed through multiple experimental trials under identical conditions, while reproducibility was verified by conducting experiments on different days to account for environmental variations such as ambient temperature and solar irradiance. Sensitivity analyses were performed in numerical simulations to evaluate the impact of deviations in input parameters, such as solar irradiance profiles, on output predictions. This approach ensures the robustness of findings and strengthens the credibility of conclusions drawn about the performance improvements achieved through hydraulic buffering control methods in PV-powered membrane desalination systems.

## 4. RESEARCH RESULTS AND DISCUSSIONS

This section provides an in-depth analysis of the performance of PV-membrane systems in mitigating SI fluctuations. It is important in evaluating the effectiveness of the hydraulic buffering control method to enhance system resilience and efficiency. The results presented include steady-state threshold tests, passive (directly-coupled) experiments and controlled buffering experiments, allowing for a detailed comparison of system behaviour.

### 4.1. Steady-state Threshold Tests

As discussed in **Section 3.3.1**, steady-state threshold tests were conducted to identify the minimum operating pressure ($P_{min}$) and the optimal set operating pressure ($P_{set}$) for the PV-membrane system. These pressure threshold values are critical for ensuring the system produces quality drinking water while maintaining relatively low SEC. The results from these steady-state threshold tests are presented in **Figure 24**.

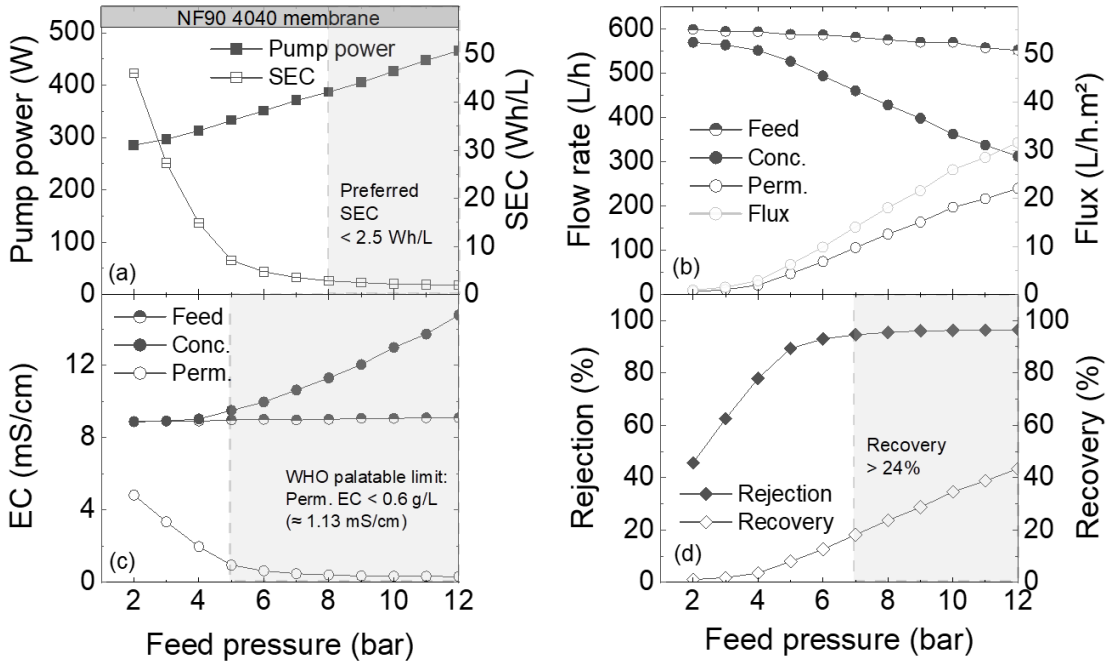

***Figure 24***. Steady-state threshold tests of the PV-membrane system: (a) Pump power consumed and SEC, (b) Flow rate and Flux, (c) EC, (d) Salt rejection and Water recovery.

The minimum operating pressure ($P_{min}$) for the PV-membrane system was identified as **8 bar**. This pressure represents the threshold at which the system achieves the preferred SEC of 2.5 Wh/L as shown in **Figure 24 (a)**, while ensuring that water quality remains within the World Health Organization (WHO) acceptable limit of EC < 0.6 g/L [59], corresponding to a conductivity of 1.13 mS/cm, as illustrated in **Figure 24 (c)**. For the NF90-4040 membrane, the preferred SEC should be less than 2.5 Wh/L. Additionally, at this operating pressure of 8 bar, the system demonstrated a salt rejection rate exceeding 90% and a water recovery rate greater than 24%, as shown in **Figure 24 (d)**, indicating that the system operates optimally at this minimum threshold, effectively balancing SEC and water quality.

Furthermore, an optimal set operating pressure ($P_{set}$) of **12 bar** was identified as the fixed operating point for all experiments (passive, uncontrolled, and controlled buffering). This pressure was selected based on the Grundfos SQF 0.6 - 2 N pump's head (the maximum height a pump can lift fluid against gravity) used for this system. At this set pressure of 12 bar, the system achieved an SEC of 1.94 Wh/L, with a permeate quality measured at an EC of 0.32 mS/cm. The system also successfully removed 96.5% of dissolved salts and produced clean drinking water at a recovery rate of 43.46%. These results demonstrate that operating at 12 bar allows the system to function efficiently while producing high-quality drinking water at a very low SEC.

4.2. Control Algorithm Flow-chart

The flow chart in **Figure 25** illustrates the control algorithm developed and implemented into the PV-membrane system to buffer periods of low SI.

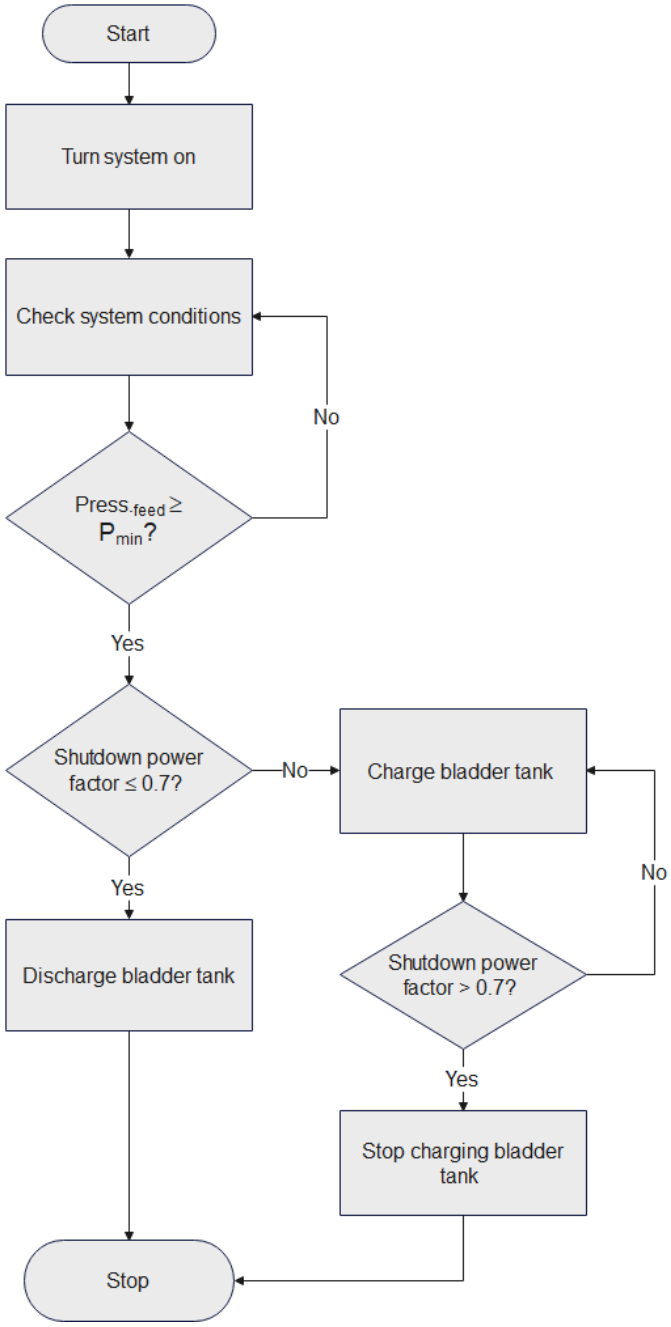


***Figure 25.*** Implemented control algorithm for pressure buffering during SI fluctuations [*Source: Author's work*]

The process begins with the initiation of the system, powering it up to commence operation, as shown in **Figure 25**. Following this, the current operating parameters of the system are verified, which involves monitoring critical factors such as feed pressure, temperature, and power availability essential for maintaining steady membrane operation. The feed pressure is evaluated to determine if it meets or exceeds the minimum required pressure of 8 bar. This step is crucial, as adequate feed pressure is required to drive water through the membrane and achieve effective permeate production. If the feed pressure falls below the threshold of 8 bar, the system will continuously recheck conditions until the minimum pressure is reached.

Once the minimum feed pressure is achieved, a subsequent check on the shutdown power factor is performed. This power factor indicates PV power fluctuations which translates to pressure fluctuations within the system. A power factor $\leq 0.7$ indicates a PV power fluctuation. In such cases, the bladder tank is discharged to stabilise pressure fluctuations and maintain flow. Conversely, if the power factor is $>0.7$, the bladder tank is charged to store additional energy or pressure in the system, ensuring continuous operation despite fluctuations.

The system remains in a loop where it continuously monitors the shutdown power factor. Should it drop below 0.7 again, the process returns to discharging the bladder tank to stabilise the system pressure. Once the power factor is consistently above this threshold, charging of the bladder tank ceases, allowing the system to proceed with normal operations. The flowchart in **Figure 25** outlines a systematic approach to managing energy

efficiency and operational stability within PV-powered membrane systems, ensuring effective water purification processes in varying solar conditions.

4.3. Passive (Directly-Coupled) and Controlled Buffering Experiments

Passive (directly-coupled) experiments were conducted to determine the pump shutdown pressure in relation to SI fluctuations. The energy consumption, pump utilisation, system losses and system efficiency were assessed and analysed in these experiments. After implementing the control algorithm, controlled buffering experiments were performed to assess the system's performance and ability to prevent pressure drops during SI fluctuations.

**Figure 26** shows the performance of the PV-membrane system on a very cloudy day, comparing results before and after the implementation of the control algorithm.

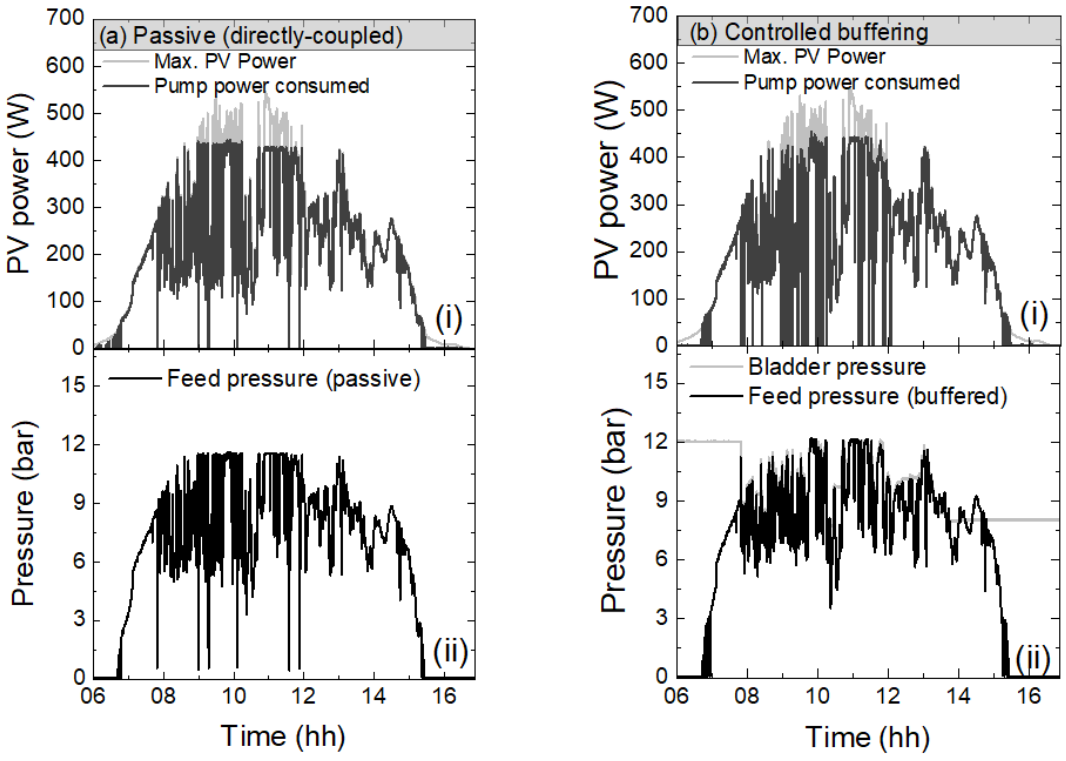


***Figure 26***. System performance of the PV-membrane system on a very cloudy day: **(a)** Passive (directly-coupled) experiment; (i) PV power supply and usage, (ii) Feed pressure, **(b)** Controlled buffering experiments; (i) PV power supply and usage, (ii) Bladder tank pressure and Feed pressure.

Significant pressure drops, reaching as low as 0.6 bar (**Figure 26 (a)(ii))**, were observed when the power output of the PV panel dropped to zero (**Figure 26 (a)(i))**. These pressure drops occurred at several intervals (07:49, 09:00, 09:17, 10:06, 11:34, and 11:52) throughout the morning due to cloud cover that limited adequate SI from reaching the PV panels, resulting in insufficient power to operate the DC pump. The Grundfos DC pump requires a minimum of 198 W to initiate operation (**Figure 21**), therefore, when the power supply was inadequate, it led to a drop in feed pressure.

After implementing the control algorithm in the control buffering experiments (**Figure 26 (b)**), no feed pressure drops were observed (**Figure 26(b)(ii)**) despite instances of pump shutdowns. This improvement is attributed to the bladder tank's ability to provide additional pressurised feedwater by discharging when a shutdown power factor below 0.7 is detected through the control algorithm. Once the system recognises a power factor above this threshold, charging of the bladder tank resumes (**Figure 26 (b)(ii)** bladder pressure graph), effectively stabilising system pressure. These findings indicate that the PV-membrane system can reliably produce clean drinking water throughout the day, demonstrating resilience against fluctuations in SI. While the system was able to produce clean drinking water continuously, it was observed that there was an increase in the number of pump shutdowns (**Figure 26 (b)(i)**) after the implementation of the control algorithm. This can be attributed to the introduction of additional pressure into the system when the bladder tank discharges, resulting in pressure difference between system and feed pressure, which the pump must overcome. However, the pump shuts down entirely due to insufficient power available to meet this increased demand. This observation

highlights the need for further optimisation of system parameters to balance pressure management and energy efficiency effectively.

**Figure 27** shows the performance of the PV-membrane system on a very cloudy day, comparing results before and after the implementation of the control algorithm.

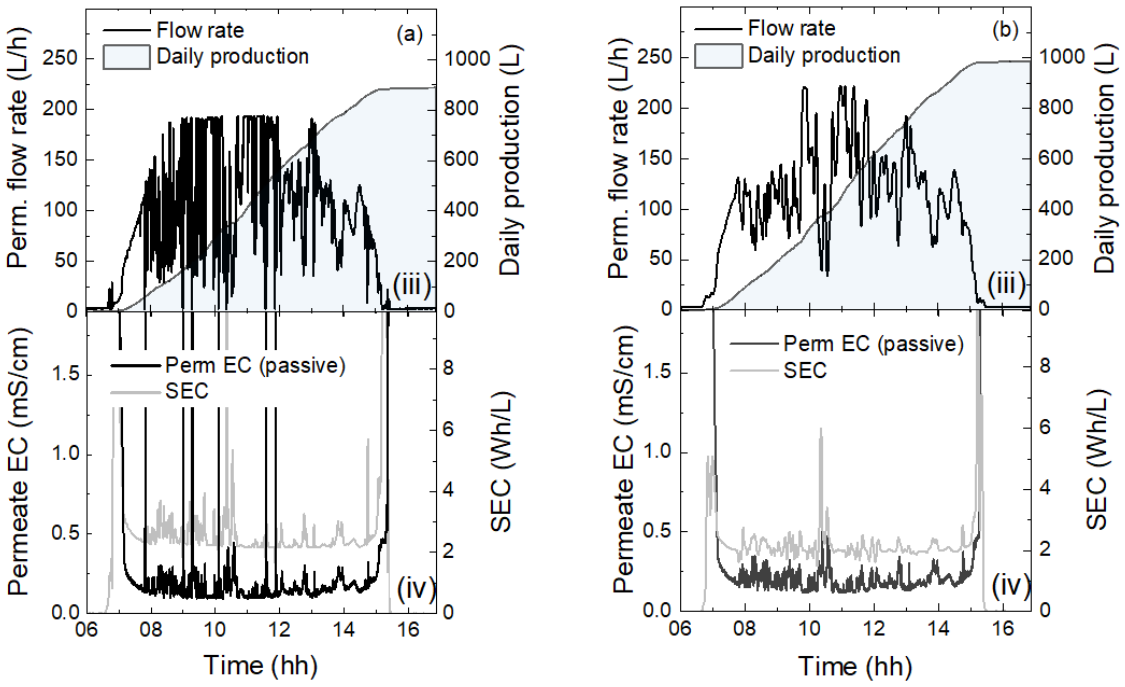


***Figure 27***. System performance of the PV-membrane system on a very cloudy day: (a) Passive (directly-coupled) experiment; (iii) Permeate flow rate and Daily water production, (iv) Permeate EC and SEC, (b) Controlled buffering experiments; (iii) Permeate flow rate.

The results presented in **Figure 27 (a)(iii)** and **Figure 27 (b)(iii)** indicates a notable increase in the maximum permeate flow rate of the PV-membrane system, rising from 190 L/h to 220 L/h following the implementation of the control algorithm. This increase in flow rate directly contributed to an increased daily production of clean drinking water, yielding an additional permeate volume of 98.5 L. The increase in permeate flow rate was

achieved as the system sustained a constant system pressure, resulting in a higher flow rate. Such findings demonstrate that the PV-membrane system is capable of continuous operation despite fluctuations in SI while producing a greater volume of permeate than the directly-coupled system.

Moreover, after implementing the buffering control, the system recorded average permeate EC and SEC values of 0.4 mS/cm and 2.4 Wh/L, respectively, significantly improving from the previous values of 0.5 mS/cm and 6.5 Wh/L. Although there was only a slight change in average permeate EC of 0.1 mS/cm, both values remained well below the WHO palatable limit of 1.13 mS/cm, indicating that water quality was effectively maintained. Importantly, achieving a lower SEC below 2.5 Wh/L reflects an enhanced energy efficiency of the system.

**Table 2** summarises the performance metrics of the PV-membrane system under both directly-coupled and controlled buffered conditions on a very cloudy day.

***Table 2***. Summary of the system performance of the PV-membrane system on a very cloudy day before and after control algorithm implementation: Maximum permeate flow rate, Daily production, Average permeate EC, and Average SEC.

| | Passive (directly-coupled) | Controlled buffering |
|---|---|---|
| Maximum permeate flow rate (L/h) | 190 | 220 |
| Daily production (L) | 890.6 | 989.1 |
| Average permeate EC (mS/cm) | 0.5 | 0.4 |

| | | |
|---|---|---|
| Average SEC (Wh/L) | 6.5 | 2.4 |

**Figure 28** shows the performance of the PV-membrane system on a very cloudy day, comparing results before and after the implementation of the control algorithm.

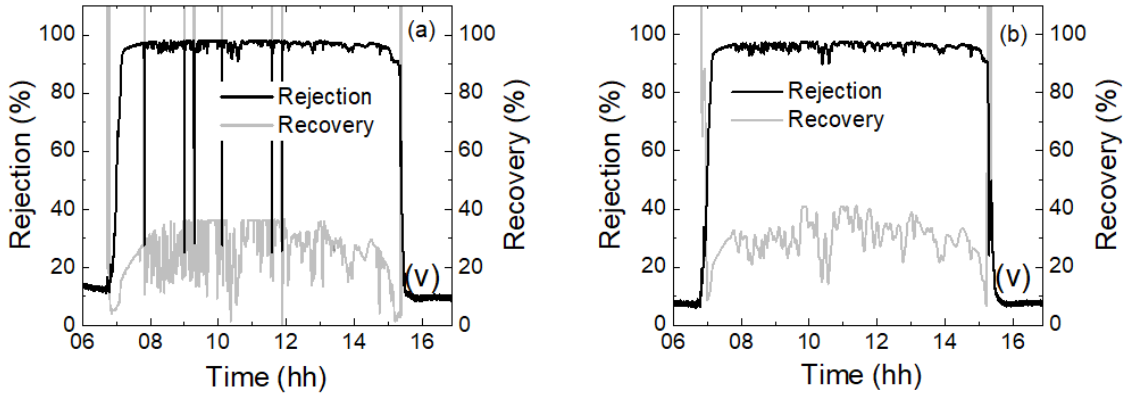


***Figure 28***. System performance of the PV-membrane system on a very cloudy day: (a) Passive (directly-coupled) experiment; (v) Salt rejection and Water recovery, (b) Controlled buffering experiments; (v) Salt rejection and Water recovery.

As shown in **Figure 28 (a)(v)** and **(b)(v),** the system was able to sustain an average salt rejection of 97%, however, there was an increase in average water recovery from 36.4 % to 39% after the implementation of the control algorithm. The increase in water recovery is due to the increase in permeate flow rate produced by the system. These results show a good performance as the PV-membrane system is operating within the preferred limits of salt rejection > 90% and water recovery > 24%.

The system was able to sustain an average salt rejection of 97%, as shown in **Figure 28 (a)(v)** and **(b)(v)**. Additionally, following the implementation of the control algorithm,

there was a notable increase in average water recovery, rising from 36.4% to 39%. This improvement in water recovery is due to increased permeate flow rate. These results indicate a good performance of the PV-membrane system, as it operates well within the preferred limits, achieving a salt rejection rate greater than 90% and a water recovery rate exceeding 24%. The ability to maintain such high levels of salt rejection while simultaneously increasing water recovery highlights the system's efficiency and effectiveness in producing potable water.

**Table 3** summarises the performance metrics of the PV-membrane system under both directly-coupled and controlled buffered conditions on a very cloudy day.

***Table 3***. Summary of the system performance of the PV-membrane system on a very cloudy day before and after control algorithm implementation: Average salt rejection and Average water recovery.

| | Passive (directly-coupled) | Controlled buffering |
|---|---|---|
| Average salt rejection (%) | 97.6 | 97.7 |
| Average water recovery (%) | 36.4 | 39 |

The results demonstrated significant improvements in water recovery and permeate quality following the implementation of the hydraulic buffering system and control algorithm. These enhancements can be directly attributed to key experimental design choices, specifically the integration of a hydraulic bladder tank and the development of a control algorithm tailored to buffer SI fluctuations. The bladder tank effectively stored

excess energy as pressurised water during periods of high SI and discharged it during low SI, ensuring stable feed pressure to the membrane. This design choice prevented pressure drops that would otherwise compromise permeate quality and water production rates. Additionally, the control algorithm monitored power ramp-down rates and dynamically adjusted the operation of the bladder tank, optimising pressure regulation and minimising pump shutdowns caused by increased resistance. These experimental design elements were critical in achieving consistent system performance under variable SI conditions, demonstrating their practical significance in improving water recovery and permeate quality in PV-powered membrane desalination systems.

Similar to the very cloudy day, passive (directly-coupled) and controlled buffering experiments were conducted on a partly cloudy day (26 May 2016) to evaluate the performance of the PV-membrane system as well as the effectiveness of the implemented control algorithm.

**Figure 29** shows the performance of the PV-membrane system on a partly cloudy day, comparing results before and after the implementation of the control algorithm.

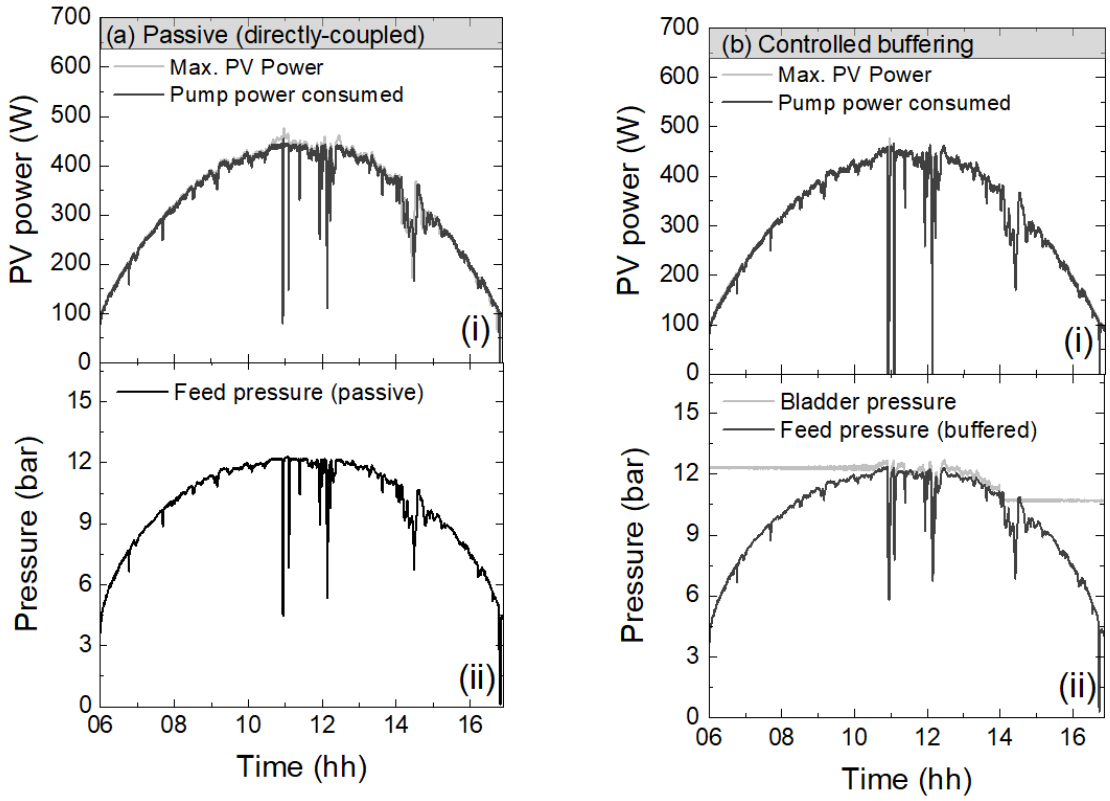


***Figure 29***. System performance of the PV-membrane system on a partly cloudy day: **(a)** Passive (directly-coupled) experiment; (i) PV power supply and usage, (ii) Feed pressure, **(b)** Controlled buffering experiments; (i) PV power supply and usage, (ii) Bladder tank pressure and Feed pressure.

As shown in **Figure 29 (a)(ii)** the system experienced a drop in feed pressure to a minimum value of 4.4 bar before the implementation of the control algorithm. This decline

occurred when the power supplied by the PV panels dropped below the critical threshold of 198 W, as illustrated in **Figure 29 (a)(i)**. The pressure drops were recorded at specific times: 10:55, 11:05, 12:09, and 14:29. These instances correspond to periods of cloud cover that limited sufficient SI from reaching the PV panels, resulting in insufficient power to drive the pump and consequently causing a reduction in the feed pressure of the system.

Following the implementation of the control algorithm, a marked improvement in feed pressure stability was observed, with a minimum value recorded at 6.1 bar, as shown in **Figure 29 (b)(ii)**. The increase in pressure is due to the additional pressurised feedwater supplied by the bladder tank during its discharge phase, which effectively buffered pressure fluctuations within the system. These results demonstrate that the PV-membrane system can continuously produce clean drinking water throughout the day, despite variations in SI, thereby confirming its reliability and resilience to such fluctuations. Furthermore, this indicates that the developed control algorithm is effective across different solar conditions.

However, it is important to note that while the system successfully maintained continuous water production, there was an increase in pump shutdown after implementing the control algorithm, as illustrated in **Figure 29 (b)(i)**. This increase can be explained by the additional pressure introduced into the system when the bladder tank discharges creating a pressure differential between the system pressure and the feed pressure, leading to pump shutdowns as it attempts to adjust and overcome this added pressure by drawing more power from the PV panels. Overall, these findings highlight the effectiveness of hydraulic

buffering in enhancing system performance and the need for further optimisation to minimise pump shutdowns during buffering periods.

**Figure 30** shows the performance of the PV-membrane system on a partly cloudy day, comparing results before and after the implementation of the control algorithm.

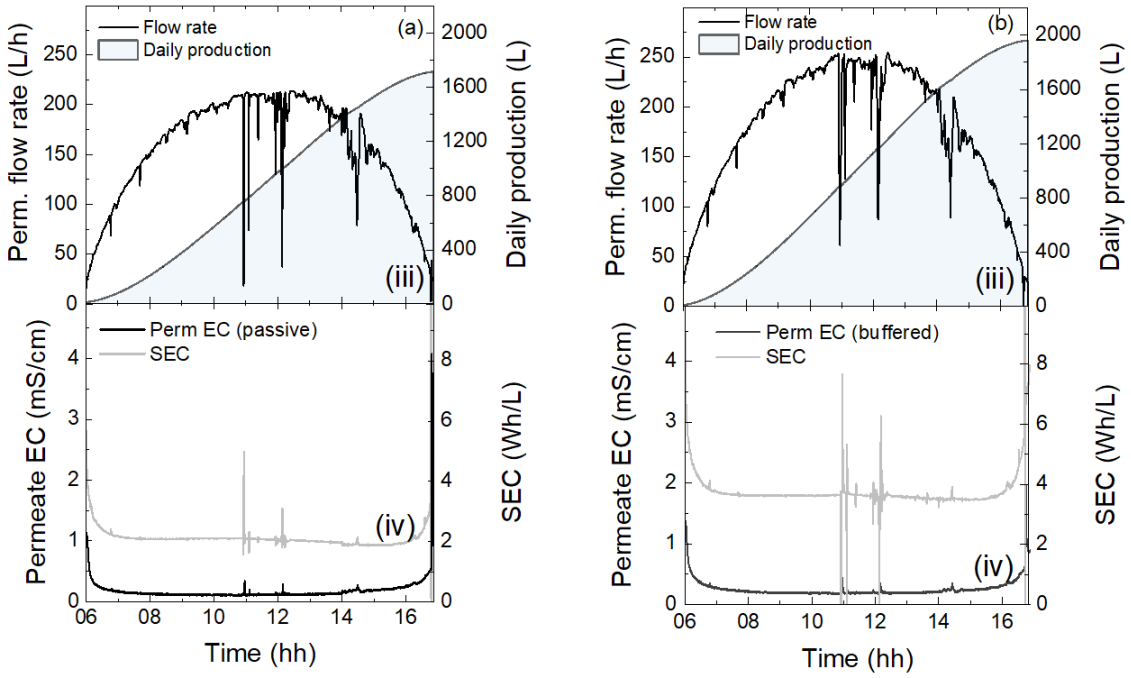


***Figure 30***. *S*ystem performance of the PV-membrane system on a partly cloudy day: (a) Passive (directly-coupled) experiment; (iii) Permeate flow rate and Daily water production, (iv) Permeate EC and SEC, (b) Controlled buffering experiments; (iii) Permeate flow rate.

The maximum permeate flow rate increased from 230 L/h to 250 L/h after implementing the control algorithm, resulting in an additional 239 L of clean drinking water produced daily as shown in **Figure 30 (a)(iii)** and **Figure 30 (b)(iii)** . This indicates that the PV-membrane system can operate continuously despite SI fluctuations and outperforms the directly-coupled system. Additionally, after buffering control, the system recorded

average permeate EC and SEC values of 0.1 mS/cm and 1.9 Wh/L, down from 0.3 mS/cm and 2.2 Wh/L respectively. The average permeate EC improved only slightly by 0.2 mS/cm, but despite the marginal improvement, permeate conductivities before and after control algorithm implementation remain below the WHO palatable limit of 1.13 mS/cm, demonstrating significant performance improvement with a lower SEC of under 2.5 Wh/L.

**Table 4** summarises the performance metrics of the PV-membrane system under both directly-coupled and controlled buffered conditions on a partly cloudy day.

***Table 4***. Summary of the system performance of the PV-membrane system on a partly cloudy day before and after control algorithm implementation: Maximum permeate flow rate, Daily production, Average permeate EC, and Average SEC.

| | Passive (directly-coupled) | Controlled buffering |
|---|---|---|
| Maximum permeate flow rate (L/h) | 230 | 250 |
| Daily production (L) | 1726.7 | 1965.7 |
| Average permeate EC (mS/cm) | 0.3 | 0.1 |
| Average SEC (Wh/L) | 2.2 | 1.9 |

**Figure 31** shows the performance of the PV-membrane system on a partly cloudy day, comparing results before and after the implementation of the control algorithm.

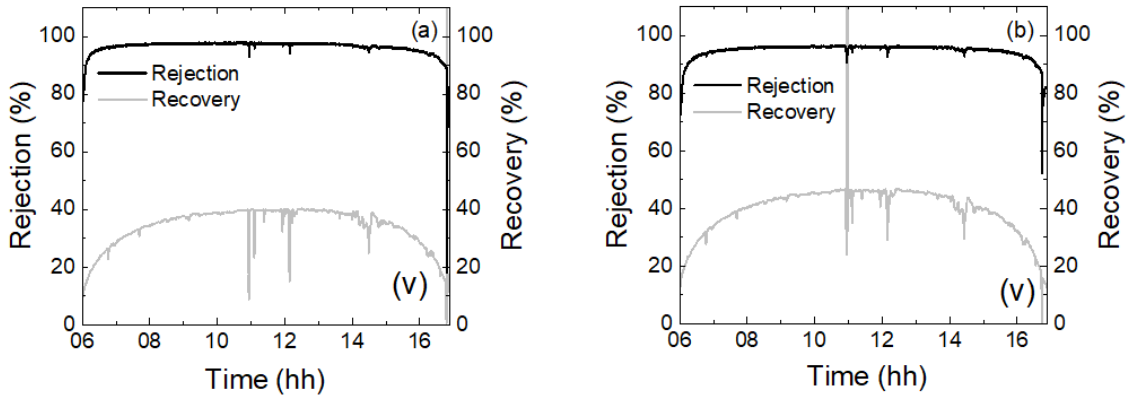


***Figure 31***. System performance of the PV-membrane system on a very cloudy day: (a) Passive (directly-coupled) experiment; (v) Salt rejection and Water recovery, (b) Controlled buffering experiments; (v) Salt rejection and Water recovery.

The system was able to sustain an average salt rejection above 95% as illustrated in **Figure 31 (a)(v)** and **(b)(v)**. However, there was a drop of 1.2% in the average salt rejection after the implementation of the control algorithm due to factors such as an increase in dissolved salts on the membrane surface. Despite the drop in average salt rejection, these results show good performance as the PV-membrane system is operating within the preferred limits of salt rejection > 90%. Additionally, there was an increase in average water recovery from 40.2 % to 46.1% after the implementation of the control algorithm due to the increase in permeate flow rate produced by the system, which still indicates a good performance of the system.

**Table 5** summarises the performance metrics of the PV-membrane system under both directly-coupled and controlled buffered conditions on a partly cloudy day.

***Table 5***. Summary of the system performance of the PV-membrane system on a partly cloudy day before and after control algorithm implementation: Average salt rejection and Average water recovery.

| | Passive (directly-coupled) | Controlled buffering |
|---|---|---|
| Average salt rejection (%) | 97.4 | 96.2 |
| Average water recovery (%) | 40.2 | 46.1 |

Passive (directly-coupled), uncontrolled buffering and controlled buffering experiments were conducted on a sunny day (5 May 2016). On this day, the weather was characterised by clear skies, which resulted in stable solar irradiance (SI) levels throughout the experimental period. Due to these favourable conditions, there were no pump shutdowns, typically occurring when solar energy production drops below operational thresholds. It is important to note that the system did not achieve any buffering during this experiment, thus keeping the bladder tank fully charged. The absence of SI fluctuations due to the clear sky meant that the hydraulic buffering system was not engaged.

# 5. CONCLUSION & RECOMMENDATIONS

## 5.1. Conclusion

The research presented in this thesis addresses a critical challenge in sustainable water solutions: the fluctuations in SI that adversely affect the performance of PV-membrane systems for water desalination. These fluctuations can lead to significant reductions in both the volume and quality of permeate water produced and an increase in specific energy consumption (SEC). The primary objective of this study was to develop a hydraulic buffering control method that would enhance the operational efficiency of PV-membrane systems during varying SI conditions. By implementing a hydraulic energy storage system utilising a bladder tank and a suitable control algorithm, the research demonstrated a novel approach to effectively buffering periods of low SI.

The findings indicate that under adverse conditions, such as during periods of low SI typically associated with cloudy weather, the system was able to produce an additional 98.5 L of permeate (11.05% increase in production) while maintaining water quality within acceptable limits established by the World Health Organization (WHO). Furthermore, the average specific energy consumption (SEC) was reduced by 38%, highlighting the effectiveness of the hydraulic buffering method. This innovative control algorithm not only facilitated energy storage during periods of high solar output but also ensured that system pressure remained stable, thereby preventing drops to zero pressure during low irradiance periods. However, certain limitations must be acknowledged to provide a balanced perspective. While the issue of pump shutdowns due to increased pressure resistance was addressed, other factors such as the long-term degradation of the

bladder tank and the sensitivity of the control algorithm to environmental changes were not explored.

This research contributes significantly to the field of renewable energy and water purification technologies, particularly in remote areas where access to clean water is a pressing issue. The successful integration of hydraulic buffering into PV-membrane systems represents a promising advancement toward achieving continuous and reliable water purification solutions. This work not only provides a pathway for improving water access but also lays the groundwork for future innovations in renewable energy applications, particularly in enhancing the resilience and sustainability of decentralized water treatment systems.

## 5.2. Recommendations

Based on the findings of this study, several recommendations are proposed for future research and practical applications. Firstly, there is a need for further optimisation of system parameters to balance pressure management and energy efficiency effectively during buffering periods, to prevent pump shutdowns. Secondly, it is advisable to conduct long-term field trials of the hydraulic buffering control system in diverse environmental conditions to validate its performance and adaptability across different geographical contexts. Such trials would provide insights into the system's resilience against varying SI patterns and operational demands. Thirdly, further exploration into alternative energy storage solutions, such as advanced hybrid systems combining multiple energy storage methods such as batteries and hydraulic accumulators, could enhance the robustness of PV-membrane systems during prolonged periods of low solar availability. Lastly, policymakers and stakeholders should consider investing in pilot projects that implement these advanced control strategies in remote communities, as this could serve as a model for scalable solutions addressing global water scarcity challenges. By fostering collaboration between researchers, engineers, and local communities, it is possible to create sustainable water infrastructure that meets immediate needs and contributes to long-term resilience against climate.

## 6. REFERENCES


[1] Schäfer A I, Hughes G and Richards B S 2014 Renewable energy powered membrane technology: A leapfrog approach to rural water treatment in developing countries? *Renewable and Sustainable Energy Reviews* **40** 542–56

[2] Anon 2021 *Progress on Household Drinking Water, Sanitation and Hygiene 2000-2020 Five Years into the SDGs* (World Health Organization)

[3] Sufiani O, Sahini M G and Elisadiki J 2023 Towards attaining SDG 6: The opportunities available for capacitive deionization technology to provide clean water to the African population *Environ Res* **216**

[4] Banat F, Jwaied N, Rommel M, Koschikowski J and Wieghaus M 2007 Desalination by a "compact SMADES" autonomous solarpowered membrane distillation unit *Desalination* **217** 29–37

[5] Al-Karaghouli A and Kazmerski L L 2013 Energy consumption and water production cost of conventional and renewable-energy-powered desalination processes *Renewable and Sustainable Energy Reviews* **24** 343–56

[6] Maftouh A, Fatni O El, Bouzekri S, Bahaj T, Kacimi I, Hajjaji S El and Malik A 2023 Solar Desalination: Current Applications and Future Potential in MENA Region – A Case Study *Journal of Sustainable Development of Energy, Water and Environment Systems* **11**

[7] Lotfy H R, Staš J and Roubík H 2022 Renewable energy powered membrane desalination — review of recent development *Environmental Science and Pollution Research* **29** 46552–68

[8] Li S, Cai Y H, Schäfer A I and Richards B S 2019 Renewable energy powered membrane technology: A review of the reliability of photovoltaic-powered membrane system components for brackish water desalination *Appl Energy* **253**

[9] Richards B S, Capão D P S, Früh W G and Schäfer A I 2015 Renewable energy powered membrane technology: Impact of solar irradiance fluctuations on performance of a brackish water reverse osmosis system *Sep Purif Technol* **156** 379–90

[10] Boussouga Y A, Richards B S and Schäfer A I 2021 Renewable energy powered membrane technology: System resilience under solar irradiance fluctuations during the treatment of fluoride-rich natural waters by different nanofiltration/reverse osmosis membranes *J Memb Sci* **617**

[11] Tzoumanikas P, Nikitidou E, Bais A F and Kazantzidis A 2016 The effect of clouds on surface solar irradiance, based on data from an all-sky imaging system *Renew Energy* **95** 314–22

[12] Woyte A, Belmans R and Nijs J 2007 Fluctuations in instantaneous clearness index: Analysis and statistics *Solar Energy* **81** 195–206

[13] Albadi M. H 2019 Solar pv power intermittency and its impacts on power systems – An overview *The Journal of Engineering Research* **16** 142–50

[14] Li S, de Carvalho A P S G, Schäfer A I and Richards B S 2021 Renewable energy powered membrane technology: Electrical energy storage options for a photovoltaic-powered brackish water desalination system *Applied Sciences (Switzerland)* **11** 1–30

[15] Li S, Voigt A, Schäfer A I and Richards B S 2020 Renewable energy powered membrane technology: Energy buffering control system for improved resilience to periodic fluctuations of solar irradiance *Renew Energy* **149** 877–89

[16] Park G L, Schäfer A I and Richards B S 2013 Renewable energy-powered membrane technology: Supercapacitors for buffering resource fluctuations in a wind-powered membrane system for brackish water desalination *Renew Energy* **50** 126–35

[17] Karavas C S, Arvanitis K G, Kyriakarakos G, Piromalis D D and Papadakis G 2018 A novel autonomous PV powered desalination system based on a DC microgrid concept incorporating short-term energy storage *Solar Energy* **159** 947–61

[18] Liu C C K, Park J, Migita R, Gang Q 2002 Experiments of a prototype wind-driven reverse osmosis desalination system with feedback control *Desalination* **150** 277–258

[19] Costa G K and Sepehri N 2023 Hydraulic accumulators in energy efficient circuits *Front Mech Eng* **9**

[20] Alonso E, Sanchez-Huerta C, Ali Z, Wang Y, Fortunato L and Pinnau I 2024 Evaluation of nanofiltration and reverse osmosis membranes for efficient rejection of organic micropollutants *J Memb Sci* **693**

[21] Nthunya L N, Bopape M F, Mahlangu O T, Mamba B B, Van der Bruggen B, Quist-Jensen C A and Richards H 2022 Fouling, performance and cost analysis of membrane-based water desalination technologies: A critical review *J Environ Manage* **301**

[22] Alluhaidan A S, Prabu P, Basheer S, Aziz R and Prakash P 2024 Integrated hybrid membrane system for enhanced water treatment and desalination for environmental preservation *Desalination Water Treat* **320**

[23] Madduri S, Sodaye H S, Debnath A K, Adak A K and Prasad T L 2023 Transformation of brackish water Reverse Osmosis membranes to nanofiltration

& ultrafiltration membranes by NaOCl treatment: Kinetic and characterization studies *Journal of Water Process Engineering* **56**

[24] The Dow Chemical Company *The Dow Chemical Company: Cleaning Procedures for DOW FILMTEC FT30 Elements*

[25] Defrance L, Jaffrin M 1999 Comparison between filtrations at fixed transmembrane pressure and fixed permeate flux: application to a membrane bioreactor used for wastewater treatment *J Memb Sci* **152** 203–10

[26] Richards B S, Capao D P S, Schäfer A I 2008 Renewable energy powered membrane technology. 2. The effect of energy fluctuations on performance of a photovoltaic hybrid membrane system *Environ Sci Technol* **42** 4563–9

[27] Field R W, Wu D, Howell J A, Gupta B B 1995 Critical flux concept for microfiltration fouling *J Memb Sci* **100** 259–72

[28] Soric A, Cesaro R, Perez P, Guiol E and Moulin P 2012 Eausmose project desalination by reverse osmosis and batteryless solar energy: Design for a 1m 3 per day delivery *Desalination* **301** 67–74

[29] Hassan Q, Jaszczur M, Abdulateef A M, Abdulateef J, Hasan A and Mohamad A 2022 An analysis of photovoltaic/supercapacitor energy system for improving self-consumption and self-sufficiency *Energy Reports* **8** 680–95

[30] Alghoul M A, Poovanaesvaran P, Mohammed M H, Fadhil A M, Muftah A F, Alkilani M M and Sopian K 2016 Design and experimental performance of brackish water reverse osmosis desalination unit powered by 2 kW photovoltaic system *Renew Energy* **93** 101–14

[31] Gür T M 2018 Review of electrical energy storage technologies, materials and systems: Challenges and prospects for large-scale grid storage *Energy Environ Sci* **11** 2696–767

[32] May G J, Davidson A and Monahov B 2018 Lead batteries for utility energy storage: A review *J Energy Storage* **15** 145–57

[33] Vega-Garita V, Hanif A, Narayan N, Ramirez-Elizondo L and Bauer P 2019 Selecting a suitable battery technology for the photovoltaic battery integrated module *J Power Sources* **438**

[34] Abu S M, Hannan M A, Hossain Lipu M S, Mannan M, Ker P J, Hossain M J and Mahlia T M I 2023 State of the art of lithium-ion battery material potentials: An analytical evaluations, issues and future research directions *J Clean Prod* **394**

[35] Fertig E and Apt J 2011 Economics of compressed air energy storage to integrate wind power: A case study in ERCOT *Energy Policy* **39** 2330–42

[36] Loudermilk C *Modeling and simulation of the dynamic effects of pressure variations on hydraulic bladder and piston style accumulators* Online: https://trace.tennessee.edu/utk_gradthes (Accessed: 16 April 2024)

[37] Epoll Hydraulic Accumulators Online: https://motorimpex.ua/files/downloads/Epoll%20Accumulators%20-%20Overview.pdf (Accessed: 16 April 2024)

[38] ATO Hydraulic Accumulators Online: https://www.ato.com/5-gallon-hydraulic-bladder-accumulator (Accessed: 17 April 2024)

[39] Chroma ATE Inc. *Programmable DC Power Supply (Solar Array Simulation) Model 62000H-S Series* Online: https://www.chromaate.com/downloads/catalogue/Power/62000H-EN.pdf (Accessed: 03 June 2024)

[40] LennTech *Dizzer P Ultrafiltration Modules* Online: https://www.lenntech.com/Data-sheets/Inge-Dizzer-P-L.pdf (02 June 2024)

[41] DuPont Water Solutions 2024 *Product Data Sheet Nanofiltration Membranes FilmTec™ NF90 Element Nanofiltration Elements for Commercial Systems* Online: https://www.dupont.com/content/dam/dupont/amer/us/en/water-solutions/public/documents/en/NF-FilmTec-NF90-PDS-45-D01520-en.pdf (Accessed: 05 May 2024)

[42] Bürkert GmbH & Co. *Pressure Measuring Device Data Sheet* Online: https://www.burkert.com/en/Media/plm/DTS/DS/ds8316-standard-eu-en.pdf?id=DTS0000000000000001000182539ENK (Accessed: 05 May 2024)

[43] Bürkert GmbH & Co. *Pressure Measuring Device Operating Manual* Online: https://www.burkert.com/en/Media/plm/MAN/MA/MA8316-Manual-EU-EN.pdf?id=MAN0000000000000001000189861EN- (Accessed: 05 May 2024)

[44] iFm Electronic Gmbh Electromagnetic Flow Sensor SM6000 Online: https://www.ifm.com/de/de/product/SM6000#details (Accessed: 02 June 2024)

[45] KOBOLD Messring GmbH *Operating Instructions for Magnetic Inductive Flowmeter Model: MIM* Online: https://www.kobold.com/Magnetic-Inductive-Flow-Meter-with-IO-Link-All-Metal-Stainless-Steel-MIM (Accessed: 02 June 2024)

[46] Bürkert GmbH & Co. *Conductivity meter, ELEMENT design* Online: https://www.burkert.com/en/Media/plm/DTS/DS/ds8222-standard-eu-en.pdf?id=DTS0000000000000001000114221ENT (Accessed: 05 May 2024)

[47] Phoenix Contact GmbH & Co. Current transducer up to 55 A, programmable and configurable Online: https://www.phoenixcontact.com/de-

de/produkte/strommessumformer-mcr-s-15-ui-dci-2814634#downloads-link-target (Accessed: 27 May 2024)

[48] OMEGA Engineering Universal Uni-/Bipolar DC Signal Transmitter Online: https://www.omega.de/pptst/DRST-DC.html#order (Accessed: 27 May 2024)

[49] Capitol Scientific Inc. LAUDA® LWG 160 Model WKL 903 Recirculating Chiller, Air Cooled, Range: -15 To 40°C, Cooling Output at 20°C: 0.8kW, Max Flow Rate: 33L/Min, 230V/50Hz Online: https://www.capitolscientific.com/LAUDA-LWG-160-Model-WKL-903-Recirculating-Chiller-Air-Cooled-Range-15-To-40C-Cooling-Output (Accessed: 05 May 2024)

[50] Goetze Group 2023 *Series 460* Online: https://www.goetze-group.com/Series/460/goetze-460-datasheet-en.pdf (27 May 2024)

[51] End Armaturen 2/2-solenoid valve, G1/2", stain. steel/NBR, 24VDC, 0-10bar, force pilot Online: https://shop.end.de/en/memg2z322245015-c (Accessed: 28 May 2024)

[52] Reflex Winkelmann GmbH *Reflex Refix DD 25, flow through expansion vessel, white, 10/4 bar* Online: https://xom-web.reflex.de/xom-rest/assets/844a5f77-bc99-4998-bf6c-f95fb7beb42c/content?locale=en (Accessed: 28 May 2024)

[53] Reflex Winkelmann GmbH *Refix Manual* Online: https://xom-web.reflex.de/xom-rest/assets/fad08e67-5625-422a-9c44-6c88767924f2/content?locale=en (Accessed: 28 May 2024)

[54] Unitronics UniStream® 10.4"- programmable logic controller with color Multi-touch HMI Online: https://www.unitronicsplc.com/unistream-series-unistream104/ (Accessed: 27 May 2024)

[55] Offgridtec *Offgridtec PCB-ETFE 100W 39V semiflexible solar panel Datasheet* Online: https://www.offgridtec.com/media/product_attachements/Datenblatt-3-01-010835-DE-EN.pdf (Accessed: 05 May 2024)

[56] Grundfos Holding SQF 0.6-2 N Online: https://product-selection.grundfos.com/products/sqflex/sqf-06-2-n-95027417?pumpsystemid=2355412058&tab=variant-specifications (Accessed: 02 June 2024)

[57] Harfington Temperature Controllers Online: https://www.harfington.com/products/p-1003582 (Accessed: 10 June 2024)

[58] OriginLab Corporation Origin 2023b Feature Highlights Online: https://www.originlab.com/2023b (Accessed: 19 April 2024)

[59] World Health Organization (WHO) 2022 *Guidelines for drinking-water quality: fourth edition incorporating the first and second addenda*

# APPENDICES

## Appendix A: Ethical Clearance Certificate

UNAM
UNIVERSITY OF NAMIBIA

### ETHICAL CLEARANCE CERTIFICATE

**Ethical Clearance Reference Number: SOS-SoS-0250** **Date: 25 OCTOBER 2024**

This Ethical Clearance Certificate is issued by the University of Namibia Ethics Committee (REC) in accordance with the University of Namibia's Research Ethics Policy and Guidelines. Ethical approval is given in respect of undertakings contained in the Research Project outlined below. This Certificate is issued on the recommendations of the ethical evaluation done by the ethics committee.

**Title of Project:** PV-POWERED MEMBRANE SYSTEM CONTROL FOR CONTINUOUS AUTONOMOUS WATER SOLUTION IN REMOTE AREAS

**Student:** RAUNA KASHEETA

**Student Number:** 201603378

**Supervisor(s):** DR. PETJA DOBREVA
PROF. BRYCE RICHARDS

**Centre for Research Services**

Take note of the following:

1. Any significant changes in the conditions or undertakings outlined in the approved Proposal must be communicated to the ethics committee. An application to make amendments may be necessary.
2. Any breaches of ethical undertakings or practices that have an impact on ethical conduct of the research must be reported to the ethics committee.
3. The Principal Researcher must report issues of ethical compliance to the ethics committee (through the Chairperson) at the end of the Project or as may be requested by the ethics committee.
4. The ethics committee retains the right to:

i) Withdraw or amend this Ethical Clearance if any unethical practices (as outlined in the Research Ethics Policy) have been detected or suspected,
ii) Request for an ethical compliance report at any point during the course of the research.

The ethics committee wishes you the best in your research.

Prof. Ezekeil Gwinyai Kwembeya (Chairperson Ethics Committee)

Prof. Davis Mumbengegwi (Head, Multidisciplinary Research)

## Appendix B: Research Permission Letter

**CENTRE FOR RESEARCH SERVICES**
*Office of the Pro-Vice Chancellor: Research, Innovation & Development*
University of Namibia, Private Bag 13301, Windhoek, Namibia
340 Mandume Ndemufayo Avenue, Pioneers Park, Office F223 - Fblock, Second Floor
☎ +264 61 206 4673; E-mail:kmbulu@unam.na; URL.: http//www.unam.edu.na

UNAM
UNIVERSITY OF NAMIBIA

**RESEARCH PERMISSION LETTER**

**Date: 04/11/2024**

**Student Name:** RAUNA KASHEETA

**Student Number:** 201603378

**Programme:** Masters of Science in Renewable Energy

**Approved Research Title:** PV-Powered Membrane System Control for Continuous Autonomous Water Solution in Remote Areas

**TO WHOM IT MAY CONCERN:**

I hereby confirm that the above-mentioned student is registered at the University of Namibia for the programme indicated. The proposed study met all the requirements as stipulated in the University guidelines and has been approved by the relevant committees.

The proposal adheres to ethical principles as per attached Ethical Clearance Certificate. Permission is hereby granted to carry out the research as described in the approved proposal.

Best Regards

**Dr. AEE Shikongo**
**Head: Postgraduate Research Support Services**
**Tel: +264 61 206 3129**
**E-mail:** aeshikongo@unam.na

CENTRE FOR RESEARCH SERVICES
Office of the Director
2024 -11- 04
University of Namibia
UNAM

## Appendix C: Experimental Starting Procedure of the PV-powered membrane in the laboratory

The procedures outlined below explain how to switch on and start the system:

### 1. Switching on all system components (excluding SAS)

1.1. Verify if the DC power supply is plugged into the AC power socket. Switch on the DC power supply by pressing the power button and inspect if it is working properly.

1.2. Inspect the entire system to verify if all the components (excluding the SAS) are powered and working properly.

1.3. Make sure that the inlet valve from the feedwater tank is open and the outlet valve is off. **NB: All valves cannot be closed or opened at the same time.**

### 2. Switching on and starting the SAS

2.1. Switch on the Solar Array Simulator (SAS) by pressing the power button.

2.2. Enter the desired voltage and current values using the SAS number keypad.

2.3. Start the SAS by pressing the **ON/OFF** button.

2.4. Lock in the values by pressing the **Lock** button to avoid tempering with the power sent to the system during operation.

### 3. Starting the system

3.1. Go to the PLC and ensure you are logged onto the homepage overview.

3.2. Select **Go to Manuals Overview**.

3.3. Select the preferred mode of system operation; directly coupled PV-membrane system or controlled mode.

3.4. Switch on the pump by selecting the **Start/stop pump** button.

3.5. Verify if the pump is switched on by checking the flow rate at any of the flow meters. The flow rate should not be 0.00.

**4. Starting the recirculating chiller**

4.1. Verify if the chiller is connected to the power supply.

4.2. Open the inlet and outlet valves of the chiller.

4.3. Switch on the chiller by pressing the power button.

4.4. Input the preferred operating temperature of the feedwater (usually between 19 ℃– 21 ℃) that will be maintained by the chiller.

**5. Data sampling**

5.1. Allow the system to run for 30 minutes to stabilize the system pressure before beginning an experiment.

5.2. Inspect if there are any leakages in the system. If so, fix the leakages.

5.3. If there are no leakages, start recording the system data after 30 minutes by selecting the Start/stop button (insert picture) on the PLC.

**Great! The system is now up and running.**

## Appendix D: Percentage of valve closure corresponding to different pressure values

**Table 6** shows different percentage values used to close the actuator valve to achieve different pressure levels in the system before starting an experiment.

***Table 6.*** Percentage valve closure

| **Pressure (bar)** | **Percentage Level (%)** |
|---|---|
| 2 | 0 |
| 3 | 38 |
| 4 | 49 |
| 5 | 55 |
| 6 | 59 |
| 7 | 62 |
| 8 | 65.5 |
| 9 | 68.5 |
| 10 | 69.5 |
| 11 | 71.5 |
| 12 | 74.3 |
| 13 | 75 |

## Appendix E: Snippets of the Hardware Configuration of the PLC and Bladder Tank Control Algorithm Implementation

# Hardware Configuration

| Property | Value |
|---|---|
| Panel Model | USP-104-B10 |
| Panel Horizontal Resolution | 800 |
| Panel Vertical Resolution | 600 |

### Local IO Units

UIA-0800N_0

| Property | Value |
|---|---|
| Number Of Analog Inputs | 8 |
| Noise Rejection | 50Hz |

| Name | Electricity Type | SW Smoothing | Enable 4 to 20 | From | To |
|---|---|---|---|---|---|
| AI8 Input 0 | 0-20mA | True | AI8_Medium | 0 | 1024 |
| AI8 Input 1 | 0-20mA | True | AI8_Medium | 0 | 1024 |
| AI8 Input 2 | 0-20mA | True | AI8_Medium | 0 | 1024 |
| AI8 Input 3 | 0-20mA | True | AI8_None | 0 | 1024 |
| AI8 Input 4 | 0-20mA | True | AI8_None | 0 | 1024 |
| AI8 Input 5 | 0-20mA | True | AI8_None | 0 | 1024 |
| AI8 Input 6 | 0-20mA | True | AI8_None | 0 | 1024 |
| AI8 Input 7 | 0-20mA | False | AI8_None | 0 | 1024 |

UIA-0800N_1

| Property | Value |
|---|---|
| Number Of Analog Inputs | 8 |
| Noise Rejection | 50Hz |

| Name | Electricity Type | SW Smoothing | Enable 4 to 20 | From | To |
|---|---|---|---|---|---|
| AI8 Input 0 | 0-20mA | True | AI8_Weak | 0 | 2047 |
| AI8 Input 1 | 0-20mA | True | AI8_Weak | 0 | 2047 |
| AI8 Input 2 | 0-20mA | True | AI8_Weak | 0 | 2047 |
| AI8 Input 3 | 0-20mA | True | AI8_None | 0 | 2047 |
| AI8 Input 4 | 0-20mA | True | AI8_None | 0 | 2048 |
| AI8 Input 5 | 0-20mA | True | AI8_None | 0 | 2048 |
| AI8 Input 6 | 0-20mA | True | AI8_None | 0 | 2048 |
| AI8 Input 7 | 0-20mA | True | AI8_None | 0 | 2048 |

UIA-0800N_2

| Property | Value |
|---|---|
| Number Of Analog Inputs | 8 |
| Noise Rejection | 50Hz |

| Name | Electricity Type | SW Smoothing | Enable 4 to 20 | From | To |
|---|---|---|---|---|---|
| AI8 Input 0 | 0-20mA | True | AI8_Weak | 0 | 1024 |
| AI8 Input 1 | 0-20mA | True | AI8_Weak | 0 | 1024 |
| AI8 Input 2 | 0-20mA | True | AI8_Weak | 0 | 1024 |
| AI8 Input 3 | 0-20mA | True | AI8_Weak | 0 | 1024 |
| AI8 Input 4 | 0-20mA | False | AI8_None | 0 | 8191 |
| AI8 Input 5 | 0-20mA | False | AI8_None | 0 | 8191 |
| AI8 Input 6 | 0-20mA | False | AI8_None | 0 | 8191 |
| AI8 Input 7 | 0-20mA | False | AI8_None | 0 | 8191 |

UIA-0800N_3

| Property | Value |
|---|---|
| Number Of Analog Inputs | 8 |
| Noise Rejection | 50Hz |

| Name | Electricity Type | SW Smoothing | Enable 4 to 20 | From | To |
|---|---|---|---|---|---|
| AI8 Input 0 | 0-20mA | True | AI8_Weak | 1024 | 0 |
| AI8 Input 1 | 0-20mA | True | AI8_Weak | 1024 | 0 |
| AI8 Input 2 | 0-20mA | True | AI8_Weak | 1024 | 0 |
| AI8 Input 3 | 0-20mA | True | AI8_Weak | 4096 | 0 |
| AI8 Input 4 | 0-20mA | True | AI8_None | 1024 | 0 |
| AI8 Input 5 | 0-20mA | True | AI8_Weak | 1024 | 0 |
| AI8 Input 6 | 0-20mA | True | AI8_Weak | 1024 | 0 |
| AI8 Input 7 | 0-20mA | True | AI8_Weak | 1024 | 0 |

UIA-0800N_4

| Property | Value |
|---|---|
| Number Of Analog Inputs | 8 |
| Noise Rejection | 50Hz |

| Name | Electricity Type | SW Smoothing | Enable 4 to 20 | From | To |
|---|---|---|---|---|---|
| AI8 Input 0 | 0-20mA | True | AI8_Weak | 0 | 1023 |
| AI8 Input 1 | 0-20mA | True | AI8_Weak | 0 | 1024 |
| AI8 Input 2 | 0-20mA | True | AI8_Weak | 0 | 1024 |
| AI8 Input 3 | 0-20mA | True | AI8_Weak | 0 | 1024 |
| AI8 Input 4 | 0-20mA | True | AI8_Weak | 0 | 1024 |
| AI8 Input 5 | 0-20mA | True | AI8_Weak | 0 | 1024 |
| AI8 Input 6 | 0-20mA | True | AI8_Weak | 0 | 1024 |
| AI8 Input 7 | 0-20mA | True | AI8_Weak | 0 | 1024 |

## UAG-XKPXXX

### UIS-WCB1_5

| Property | Value |
|---|---|
| Number Of Digital Inputs | 10 |
| Number Of Digital Outputs | 8 |
| Number Of Analog Inputs | 2 |
| Number Of Analog Outputs | 2 |
| Noise Rejection | 50Hz |
| Digital Input(0-9) Filter in msec | 8 |

| Name | Electricity Type | SW Smoothing | Enable 4 to 20 | From | To |
|---|---|---|---|---|---|
| Analog Input 0 | 0-20mA | AI8_None | True | 0 | 1024 |
| Analog Input 1 | 0-20mA | AI8_None | True | 0 | 1024 |

| Name | Sensor Type | Display Type | From | To | SW Smoothing |
|---|---|---|---|---|---|
| Temperature Input 0 (RT2) | NONE | N/A | N/A | N/A | N/A |
| Temperature Input 1 (RT3) | NONE | N/A | N/A | N/A | N/A |

| Name | From | To |
|---|---|---|
| Analog Output 0 | 0 | 1024 |
| Analog Output 1 | 0 | 1024 |

| Name | High-Speed Type |
|---|---|
| HS Block 1 | Off |

| Name | High-Speed Type |
|---|---|
| HS Block 2 | Off |

### UIS-WCB1_6

| Property | Value |
|---|---|
| Number Of Digital Inputs | 10 |
| Number Of Digital Outputs | 8 |
| Number Of Analog Inputs | 2 |
| Number Of Analog Outputs | 2 |
| Noise Rejection | 50Hz |
| Digital Input(0-9) Filter in msec | 8 |

| Name | Electricity Type | SW Smoothing | Enable 4 to 20 | From | To |
|---|---|---|---|---|---|
| Analog Input 0 | 0-20mA | AI8_None | False | 0 | 16383 |
| Analog Input 1 | 0-20mA | AI8_None | False | 0 | 16383 |

| Name | Sensor Type | Display Type | From | To | SW Smoothing |
|---|---|---|---|---|---|
| Temperature Input 0 (RT2) | NONE | N/A | N/A | N/A | N/A |
| Temperature Input 1 (RT3) | NONE | N/A | N/A | N/A | N/A |

| Name | From | To |
|---|---|---|
| Analog Output 0 | 0 | 8191 |
| Analog Output 1 | 0 | 8191 |

| Name | High-Speed Type |
|---|---|
| HS Block 1 | Off |

| Name | High-Speed Type |
|---|---|
| HS Block 2 | Off |

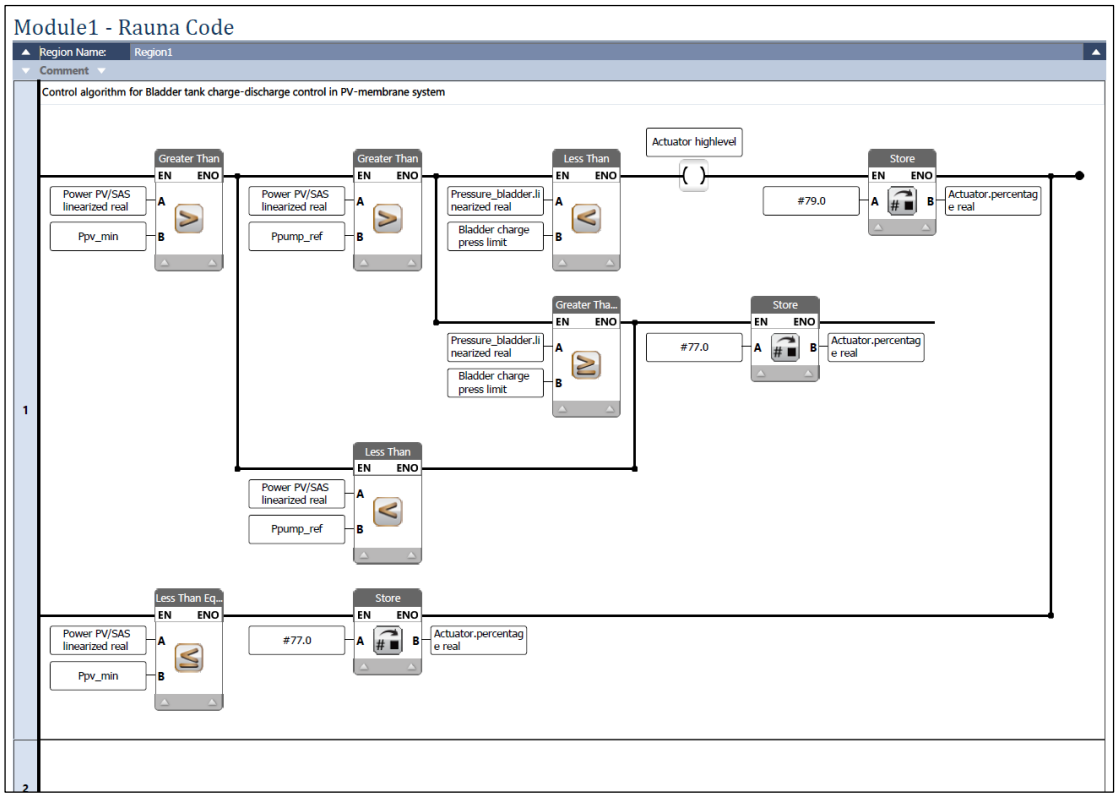
Module1 - Rauna Code
Region Name:
Region1
Comment
Control algorithm for Bladder tank charge-discharge control in PV-membrane system
1
2
Greater Than
EN
ENO
Power PV/SAS linearized real
A
Ppv_min
B
Greater Than
Power PV/SAS linearized real
Ppump_ref
Less Than
Pressure_bladder.linearized real
Bladder charge press limit
Actuator highlevel
Store
#79.0
Actuator.percentage real
Greater Tha...
#77.0
Less Than
Less Than Eq...
Ppv_min